

# LITTLEWOOD–RICHARDSON COEFFICIENTS AND INTEGRABLE TILINGS

PAUL ZINN-JUSTIN

ABSTRACT. We provide direct proofs of product and coproduct formulae for Schur functions where the coefficients (Littlewood–Richardson coefficients) are defined as counting puzzles. The product formula includes a second alphabet for the Schur functions, allowing in particular to recover formulae of [Molev–Sagan ’99] and [Knutson–Tao ’03] for factorial Schur functions. The method is based on the quantum integrability of the underlying tiling model.

## CONTENTS

1. Introduction	2
2. The tiling model	3
2.1. Tiles	3
2.2. Paths	3
3. Fock spaces	4
3.1. Fermionic Fock space $\mathcal{F}$	4
3.2. Fock space $\mathcal{G}$ of the tiling model	5
3.3. From $\mathcal{F}$ to $\mathcal{G}$	6
4. Transfer matrices	7
4.1. The transfer matrix of free fermions	7
4.2. The transfer matrix of the tiling model	9
4.3. The two families of commuting transfer matrices	10
5. Littlewood–Richardson Coefficients	12
5.1. The coproduct formula	12
5.2. Back to the triangle	13
6. Proof of the commutation theorem	14
6.1. $R$ -matrix and Yang–Baxter equation	14
6.2. The RTT relations	16
6.3. Other cases	18
7. Equivariance or the introduction of inhomogeneities	18
7.1. Factorial Schur functions	19
7.2. MS-puzzles and equivariant puzzles	20
7.3. The Molev–Sagan problem	22
7.4. Alternate solution of the Molev–Sagan problem	25
7.5. The Knutson–Tao problem	27
Appendix A. Square-triangle-rhombus tilings	27
References	29

---

The author wants to thank J. de Gier and B. Nienhuis for providing him with their unpublished work, and A. Knutson and R. Langer for encouragement and useful comments.

PZJ was supported by EU networks “ENRAGE” MRTN-CT-2004-005616, “ENIGMA” MRT-CT-2004-5652, ESF program “MISGAM” and ANR program “GIMP” ANR-05-BLAN-0029-01.

## 1. INTRODUCTION

Littlewood–Richardson coefficients are important integers related to Schur functions or equivalently to the representation theory of the general linear group; they also appear in the cohomology of Graßmannians. Interesting combinatorial formulae for them have been given in [11, 10]: these coefficients count puzzles, i.e. certain tilings of a triangle where the tiles are decorated elementary triangles and rhombi. However all the proofs of this formula are fairly indirect e.g. rely on induction.

From the mathematical physicist’s point of view, Littlewood–Richardson coefficients provide a challenge. It is well-known [7] that Schur functions are related to (two-dimensional) *free fermions*. However it is not clear how to define Littlewood–Richardson coefficients in this framework. In fact the construction of [10], as will be discussed here, suggests that the right way to describe them involves *interacting* fermions. Interestingly, the physical model in question has in fact been studied in the physics literature. As pointed out in [16], it is equivalent to a model of *random tilings*, the square-triangle triangle model, which has been the subject of a lot of activity [17, 8, 1]. Note that this equivalence is not particularly useful – in order to solve the square-triangle tiling model, one usually goes back to the model of tilings of decorated triangles and rhombi. The most important feature of this model for our purposes is that it is *integrable*: the scattering of the elementary degrees of freedom (the aforementioned interacting fermions) is factorized and thus satisfies the Yang–Baxter equation (with spectral parameters).

A general consequence of integrability is the existence of a commuting family of transfer matrices that contains the original transfer matrix describing the discrete time evolution of the system. In the case of free fermions, these transfer matrices precisely “grow” Schur functions. Here we find in fact two families of commuting matrices [2]. It is quite satisfying that computing their matrix elements naturally produces one of the expressions that define Littlewood–Richardson coefficients, namely the *coproduct* formula. We thus obtain a direct proof of the combinatorial formula for them.

Furthermore, the integrability strongly suggests to introduce arbitrary spectral parameters into the model: this corresponds to extending the original tiling model to a more general inhomogeneous model. This naturally produces generalizations of the Littlewood–Richardson coefficients which are polynomials of the inhomogeneities. We recover this way several known formulae [10, 15] as well as a new one for the coefficients in the expansion of the *product* of factorial (or double) Schur functions.

The paper is organized as follows. Section 2 is a presentation of the tiling model which will be used throughout this paper. Sections 3 and 4 present the main ingredients in the derivation of the coproduct formula: the Fock space/transfer matrix formalism. Section 5 is the derivation itself, and section 6 contains the proof of the main theorem used in section 5. Finally, section 7 describes the inhomogeneous model and its application to product formulae for factorial Schur functions. The appendix briefly discusses the equivalence to a square-triangle-rhombus tiling model.

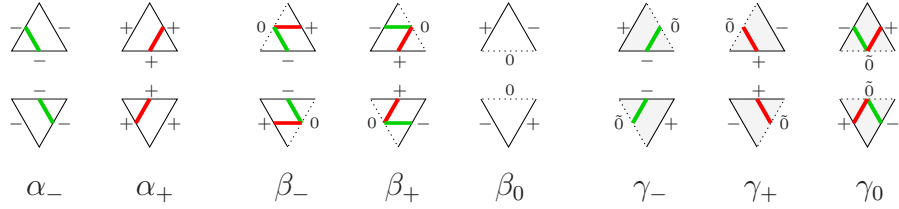
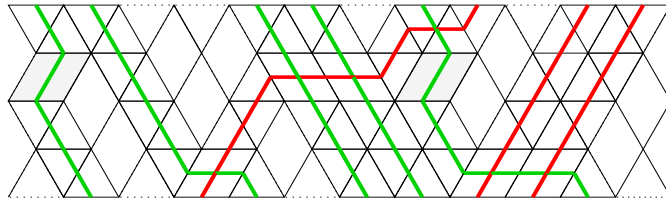


FIGURE 1. The tiles.

FIGURE 2. An example of tiling, using tiles  $\alpha_{\pm}$ ,  $\beta_{\pm 0}$ ,  $\gamma_-$ .

## 2. THE TILING MODEL

We provide here our own formulation of the model of tilings by decorated rhombi and triangles which is the basis of [10] (we actually extend it slightly by defining two additional tiles).

**2.1. Tiles.** The model is defined by filling a domain contained inside the triangular lattice with tiles of the form shown on Fig. 1. More precisely, one can use *either* the colored lines inside the tiles *or* the symbols on the edges to decide if adjacent tiles match: that is, symbols must coincide on the edges, or equivalently green and red lines must propagate across edges. Colored lines or edge labels can be thought of as two equivalent ways to encode the four possible states of edges, which each have their advantages. We shall mostly use colored lines in what follows. The correspondence of edge labels with the notation of [10] is  $- \leftrightarrow 0$ ,  $+ \leftrightarrow 1$ ,  $0 \leftrightarrow 10$ ,  $\bar{0} \leftrightarrow 01$ . The shading of the tiles  $\gamma$  will be explained later (cf a similar shading in [10]).

Note that we have classified tiles in pairs; this is because the two tiles of type  $\beta_-$ ,  $\beta_+$ ,  $\beta_0$ ,  $\gamma_-$ ,  $\gamma_+$ ,  $\gamma_0$  always appear together on adjacent triangles to form rhombi, which we have illustrated by using dotted lines. There is some freedom however in how to reconnect the two tiles of type  $\alpha_{\pm}$ : an upper tile of type  $\alpha_-$  can have on its left any number of pairs of tiles of type  $\beta_+$ ; the only way this series can end is with a lower tile of type  $\alpha_-$ . Similarly for the tiles of type  $\alpha_+$ , with series of tiles of type  $\beta_-$  on its right. In what follows it will be convenient to consider tilings of the whole plane. However, we shall see that with our “boundary conditions” (conditions at left and right infinity), all such series of tiles of type  $\beta_{\pm}$  will be necessarily finite.

**2.2. Paths.** At this stage we can forget about the underlying triangles and rhombi and simply keep track of the paths formed by the green and red lines. Consider a horizontal line in the triangular lattice. Each edge can be in only three states: empty or occupied by a green or red line. In what follows we shall number edges using alternatingly half-odd-integers and

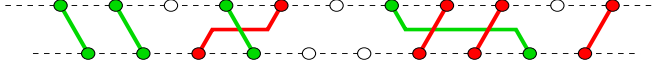


FIGURE 3. An example of evolution of paths from one time step to the next.

integers to take into account the nature of the lattice. (One could of course get rid of this issue by applying an additional shift by a half-step say to the right, but that would break the left-right symmetry of the model, and we do not choose to do so here.)

We now analyze what happens to the lines during one “time step”, that is as one moves (upwards) from one horizontal line to the next. Let us first ignore the tiles  $\gamma_{0,-,+}$ . This corresponds to the original tiling model of [17] which also occurs in [10] (in the non-equivariant case). Then the rules are as follows: a green (resp. red) line moves one half-step to the right (resp. left) if there is currently no particle of the opposite kind at this spot. The only situation left to consider is when lines of opposite colors are adjacent, with the green line at the left. Then two scenarios occur: either the green line crosses all the red lines at its right until it finds an empty spot, or the red line crosses all the green lines at its left until it finds an empty spot. This is shown on Fig. 3.

If we add the tiles  $\gamma_-$  (resp.  $\gamma_+$ ), then green (resp. red) lines have the additional possibility of moving in the opposite direction as normally, on condition that the spot is free. If we add the tile  $\gamma_0$ , then green and red lines are allowed to simply cross each other as if they did not see each other.

### 3. FOCK SPACES

For our purposes it is necessary to encode the possible configurations on a given horizontal line into a Hilbert space. But first we describe a slightly simpler space (only two states per site instead of three) which will play an important role.

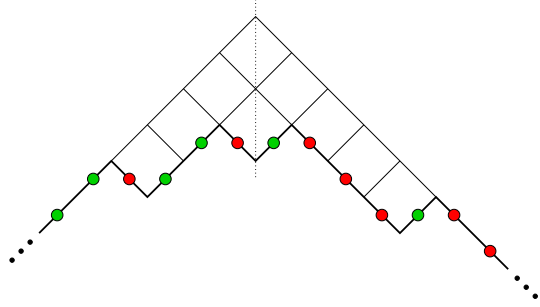
**3.1. Fermionic Fock space  $\mathcal{F}$ .** The Fock space  $\mathcal{F}$  is an infinite dimensional Hilbert space with canonical orthonormal basis defined as follows. Each element  $|f\rangle$  of the basis is indexed by a map  $f$  from  $\mathbb{Z} + \frac{1}{2}$  to  $\{-1, 1\}$  such that there exists  $N_-$ ,  $N_+$  such that  $f(i) = -1$  for  $i < N_-$  and  $f(i) = +1$  for  $i > N_+$ . Call  $N_+(f)$  (resp.  $N_-(f)$ ) the smallest (resp. largest) such integer.

We shall represent the  $-1$ 's (resp.  $1$ 's) as green (resp. red) particles or dots.

There is a notion of “charge” which can be thought of as follows: each green particle has charge  $-1$  and each red particle has charge  $+1$ . This is ill-defined because there is an infinite number of particles, so we need a reference state. Define  $|\emptyset\rangle$  (the vacuum state) to be the state such that there are only green particles to the left of zero and only red particles to the right. The corresponding map from  $\mathbb{Z} + \frac{1}{2}$  to  $\{-1, 1\}$  is the sign map.  $|\emptyset\rangle$  has by definition zero charge. This way, the charge of any state  $|f\rangle$  is given by  $c(f) := \sum_{i \in \mathbb{Z} + \frac{1}{2}} (f(i) - \text{sign}(i))$ . The charge is always an even number (we use twice the standard convention, for reasons that will become clear).

Define the shift operator  $\mathbf{S}$ : it is defined by  $\mathbf{S}|f\rangle = |f'\rangle$  with  $f'(i+1) = f(i)$  for all  $i$ .  $\mathbf{S}$  decreases the charge by 2, and is an isomorphism between subspaces of different charge.

It is well-known [7] (see also [18]) that in a subspace of given charge, basis elements can alternatively be indexed by Young diagrams. The correspondence goes as follows. Rotate the Young diagram 45 degrees, assign green dots and red dots to edges of either orientation as indicated on the picture:



One can then flatten the line and obtain a configuration of green and red dots. There remains the arbitrariness in shifting the line, or equivalently in the charge. Here we shall only consider the case of zero charge, in which case the convention is that the diagonal line (dotted line on the picture) represents the zero. In such a way to any Young diagram  $\lambda$  we associate a state simply denoted by  $|\lambda\rangle$ , and all the basis vectors of the subspace with zero charge are recovered this way. In the case of the empty diagram we recover our vacuum state  $|\emptyset\rangle$ .

Finally, define for future use  $\mathcal{F}_{+,k}$  (resp.  $\mathcal{F}_{-,k}$ ) to be the span of the  $|f\rangle$  such that  $N_+(f) \leq k$  (resp.  $N_-(f) \geq -k$ ).

**3.2. Fock space  $\mathcal{G}$  of the tiling model.** The Fock space  $\mathcal{G}$  can be similarly described as follows. Basis vectors  $|f\rangle$  of  $\mathcal{G}$  are indexed by maps  $f$  from  $\mathbb{Z} + \frac{1}{2}$  to  $\{-1, 0, +1\}$  such that there exists  $N_-, N_+$  such that  $f(i) = -1$  for  $i < N_-$  and  $f(i) = +1$  for  $i > N_+$ .

The correspondence to configurations of the tiling model described in the previous section is as follows: each basis vector of  $\mathcal{G}$  encodes a horizontal line in a configuration of tiles; thus,  $-1 \equiv -$  correspond to a green particle,  $0$  to an empty spot and  $+1 \equiv +$  to a red particle. Since the model is translationally invariant the choice of an origin is irrelevant; however, note that successive lines have all sites shifted by half a step, which means that  $\mathcal{G}$  can only describe rows of a given parity, not both at the same time. We shall come back to this point below.

Define  $N_{\pm}(f)$  similarly as before: that is,  $N_-(f)$  is the location of the leftmost empty spot or red particle minus one half, whereas  $N_+(f)$  is the location of the rightmost empty spot or green particle plus one half. We can also define two more numbers which will be useful:  $N_{-0}(f)$  is the location of the leftmost red particle minus one half, whereas  $N_{+0}(f)$  is the location of the rightmost green particle plus one half.

There are two “quantum numbers” in  $\mathcal{G}$ . The first one, the charge, is defined in  $\mathcal{G}$  as in  $\mathcal{F}$  by  $c(f) := \sum_{i \in \mathbb{Z} + \frac{1}{2}} (f(i) - \text{sign}(i))$  i.e. green particles have charge  $-1$ , red particles have charge  $+1$ , empty spots have zero charge. The charge is an integer with arbitrary parity.

The second quantum number, the “emptiness number”, is simply the number of zeroes:  $e(f) := \#\{i : f(i) = 0\}$ .

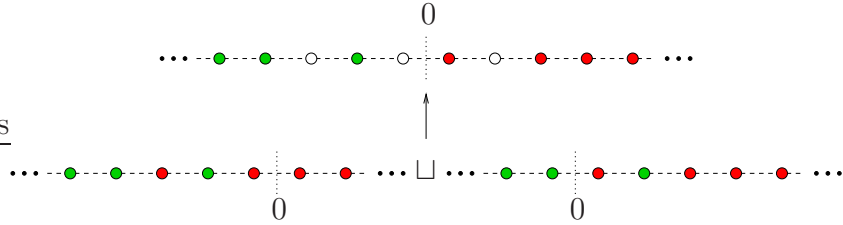


FIGURE 4. The concatenation map.

Intuitively, the conservation of the two quantum numbers is related to the conservation of the number of lines of either color in any finite region. Since we have an infinite system, particles can however “leak to infinity”, which results in variation of these quantum numbers.

There is again a shift operator, denoted by  $\mathbf{S}$ , which to  $|f\rangle \in \mathcal{G}$  associates  $|f'\rangle$  such that  $f'(i+1) = f(i)$  for all  $i$ .  $\mathbf{S}$  preserves the emptiness number, and decreases the charge by 2.

### 3.3. From $\mathcal{F}$ to $\mathcal{G}$ .

There are two types of maps we need to define from  $\mathcal{F}$  to  $\mathcal{G}$ .

There is the obvious inclusion map from  $\mathcal{F}$  to  $\mathcal{G}$ . This identifies  $\mathcal{F}$  with the subspace of  $\mathcal{G}$  with zero emptiness number.

The less obvious map  $\sqcup$  takes two basis elements  $|f_-\rangle$  and  $|f_+\rangle$  and produces  $|f\rangle = |f_-\rangle \sqcup |f_+\rangle$  in  $\mathcal{G}$  such that

$$f(i) = \begin{cases} \frac{1}{2}(f_-(i) - 1) & i < 0 \\ \frac{1}{2}(f_+(i) + 1) & i > 0 \end{cases}$$

In other words it “concatenates” the two words by discarding the right of  $f_-$  and the left of  $f_+$ .

More generally, define for  $k \in \mathbb{Z}$

$$|f_-\rangle \sqcup_k |f_+\rangle = \mathbf{S}^{-k} |f_-\rangle \sqcup \mathbf{S}^k |f_+\rangle$$

This map  $\sqcup_k$  is injective if one restricts to  $|f_-\rangle$  and  $|f_+\rangle$  such that  $N_+(f_-) \leq k$  and  $N_-(f_+) \geq -k$ , which is the only situation where we shall use  $\sqcup_k$ . We thus consider from now on  $\sqcup_k$  as a linear map from  $\mathcal{F}_{+,k} \otimes \mathcal{F}_{-,k}$  to  $\mathcal{G}$ .

It is an easy calculation that if  $|f\rangle = |f_-\rangle \sqcup_k |f_+\rangle$ ,

$$\begin{aligned} c(f) &= \frac{1}{2}(c(f_-) + c(f_+)) \\ e(f) &= \frac{1}{2}(c(f_-) - c(f_+)) + 2k \end{aligned}$$

The image of  $\sqcup_k$ , denoted by  $\mathcal{G}_{\text{free}} \subset \mathcal{G}$ , is exactly the span of the  $|f\rangle$  such that  $N_{-0}(f) \geq 0$  and  $N_{+0}(f) \leq 0$ .

*Remark 1:* intuitively, this second operation has the following meaning. When the sets of green and red particles are widely separated from each other (green ones being on the left and red ones on the right), then each of them behaves like a system of fermions (the fermionic character being the condition that there can be at most one particle per site).

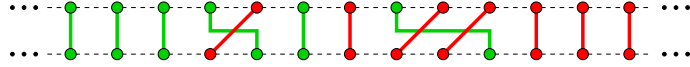


FIGURE 5. An example of evolution of the free fermionic model.

#### 4. TRANSFER MATRICES

We should be a little careful what we mean by a “transfer matrix” here because of the fact that we are dealing with infinite-dimensional spaces. A transfer matrix is defined here as a matrix, that is a collection of entries  $(\mathbf{T}_{f,g})$  where  $f$  and  $g$  index the canonical basis of  $\mathcal{F}$  or  $\mathcal{G}$ . It is tempting to associate to it a linear operator  $\mathbf{T}$  on  $\mathcal{F}$  or  $\mathcal{G}$ , such that  $\mathbf{T}_{f,g} = \langle f | \mathbf{T} | g \rangle$ , but this is problematic because sometimes the action of  $\mathbf{T}$  leads to an infinite linear combination of basis elements, which would require discussing the convergence of summations. However in all that follows, whenever we have two transfer matrices  $\mathbf{T}$  and  $\mathbf{T}'$ , the product  $(\mathbf{T}\mathbf{T}')_{f,h} = \sum_g \mathbf{T}_{f,g} \mathbf{T}'_{g,h}$  only involves finite sums and is therefore well-defined; so that we can safely ignore this subtlety and manipulate transfer matrices as operators.

**4.1. The transfer matrix of free fermions.** We first define the usual dynamics for free fermions that leads to Schur functions, see e.g. [18].

The transfer matrix, denoted by  $\mathbf{T}_{\text{free}}(u)$ , is most simply described by considering red dots as lines propagating (similarly as green and red lines in the tiling model). In this case the rule of evolution for red lines is that at each step, they can either move straight upwards or upwards and one step to the right on condition that no two lines touch each other. An example is given on Fig. 5. Furthermore, sufficiently far to the right, we impose that red lines go straight upwards. This way any evolution only involves finitely many moves to the right: we then assign a weight of  $u$  to each such move. Explicitly,  $\langle f | \mathbf{T}_{\text{free}}(u) | f' \rangle$  equals the sum over configurations of the form of Fig. 5 where the initial configuration (at the bottom) is described by  $f'$  and the final configuration (at the top) is described by  $f$ , of  $u$  to the power the number of moves to the right.

One remark is in order. One can of course also assign lines to the green dots and formulate the rules in terms of the green lines (see [18] for details). These lines have also been represented on Fig. 5. The rule is that at each time step green lines can move up half-way then arbitrarily far to the left then up again, but in such a way that they do not touch any other green lines along the way. The weight of  $u$  is given to each crossing of green and red lines.

$\mathbf{T}_{\text{free}}(u)$  breaks the “particle–hole” symmetry that exchanges left and right, green and red lines, since the rules are clearly different for the two types of lines. One can therefore introduce a mirror-symmetric transfer matrix  $\overline{\mathbf{T}}_{\text{free}}(u)$ . It is defined similarly as  $\mathbf{T}_{\text{free}}(u)$ , but this time, the green lines are allowed to go either straight upwards or upwards and one step to the left. Each left move is given a weight of  $u$ .

Both  $\mathbf{T}_{\text{free}}(u)$  and  $\overline{\mathbf{T}}_{\text{free}}(u)$  preserve the charge.

Finally, we have the following important formulae:

**Lemma 1.**

$$s_{\lambda/\mu}(u_1, \dots, u_n) = \langle \mu | \prod_{i=1}^n \mathbf{T}_{\text{free}}(u_i) | \lambda \rangle$$

is the skew Schur function associated with the Young diagram  $\lambda$ . For  $\mu = \emptyset$ ,

$$s_\lambda(u_1, \dots, u_n) = \langle \emptyset | \prod_{i=1}^n \mathbf{T}_{\text{free}}(u_i) | \lambda \rangle$$

is the Schur function associated with the Young diagram  $\lambda$ . Similarly,

$$s_{\lambda^T/\mu^T}(u_1, \dots, u_n) = \langle \mu | \prod_{i=1}^n \overline{\mathbf{T}}_{\text{free}}(u_i) | \lambda \rangle$$

where  $\lambda^T$  is the transpose of  $\lambda$ , and in particular

$$s_{\lambda^T}(u_1, \dots, u_n) = \langle \emptyset | \prod_{i=1}^n \overline{\mathbf{T}}_{\text{free}}(u_i) | \lambda \rangle$$

The most general formula is

$$s_{\lambda/\mu}(u_1, \dots, u_m/v_1, \dots, v_n) = \langle \mu | \prod_{i=1}^m \mathbf{T}_{\text{free}}(u_i) \prod_{i=1}^n \overline{\mathbf{T}}_{\text{free}}(v_i) | \lambda \rangle$$

that is the supersymmetric skew Schur function, which leads for  $\mu = \emptyset$  to the usual supersymmetric Schur function

$$s_\lambda(u_1, \dots, u_m/v_1, \dots, v_n) = \langle \emptyset | \prod_{i=1}^m \mathbf{T}_{\text{free}}(u_i) \prod_{i=1}^n \overline{\mathbf{T}}_{\text{free}}(v_i) | \lambda \rangle$$

*Proof.* There are several simple proofs of this standard result. One involves a bijection between these paths and the appropriate tableaux that one uses to define supersymmetric Schur functions. Another proof, which we sketch here, is to use the Lindström–Gessel–Viennot (LGV) formula [13, 6]. We apply it to the green lines to the right of  $N_-(\lambda)$  (those to the left necessarily go straight). There are exactly  $\lambda'_1$  such lines, where  $\lambda'_1$  is the number of non-zero rows of  $\lambda$ . This leads us to compute the evolution for a single line from initial location  $k$  to final location  $k + j$ . Noting that the rules of evolution are translationally invariant, one can introduce a generating function  $h^{(i)}(x) = \sum_{j \geq 0} h_j^{(i)} x^j$  for the time step corresponding to  $\mathbf{T}_{\text{free}}(u_i)$  and  $e^{(i)}(x) = \sum_{j \geq 0} e_j^{(i)} x^j$  for the time step corresponding to  $\overline{\mathbf{T}}_{\text{free}}(v_i)$ .  $h_j^{(i)}$  and  $e_j^{(i)}$  are the numbers of ways to move  $j$  steps to the left for a single green line and a single time step, so we immediately find

$$h^{(i)}(x) = (1 - xu_i)^{-1} \quad e^{(i)}(x) = 1 + xv_i$$

Composing the transfer matrices amounts to multiplying the generating series, so we find the evolution for a single green line to be given by the generating series

$$h(x; u_1, \dots, u_m/v_1, \dots, v_n) = \frac{\prod_{i=1}^n (1 + xv_i)}{\prod_{i=1}^m (1 - xu_i)}$$

which is exactly the generating series of the supersymmetric analogues of completely symmetric functions i.e. Schur functions  $h_j$  corresponding to one row:

$$h(x; u_1, \dots, u_m/v_1, \dots, v_n) = \sum_{j \geq 0} h_j(u_1, \dots, u_m/v_1, \dots, v_n) x^j$$

Applying the LGV formula produces the Giambelli identity for supersymmetric Schur functions

$$s_{\lambda/\mu}(u_1, \dots, u_m/v_1, \dots, v_n) = \det(h_{\lambda_j - \mu_i + i - j}(u_1, \dots, u_m/v_1, \dots, v_n))_{1 \leq i, j \leq \lambda'_1}$$

□

*Remark 2:* lemma 1 implies the commutation relations

$$[\mathbf{T}_{\text{free}}(u), \mathbf{T}_{\text{free}}(v)] = 0 \quad [\mathbf{T}_{\text{free}}(u), \overline{\mathbf{T}}_{\text{free}}(v)] = 0 \quad [\overline{\mathbf{T}}_{\text{free}}(u), \overline{\mathbf{T}}_{\text{free}}(v)] = 0$$

which were apparent in the proof. They are also a consequence of the more general results of the next section.

**4.2. The transfer matrix of the tiling model.** Before defining the transfer matrix of the tiling model, one must discuss the problem of the numbering of successive rows. Since the edges are shifted by a half-step during one time unit, there are two symmetric choices: shift everything one half-step to either the right or the left (either before or after the evolution, since it is translationally invariant). The resulting transfer matrices are called respectively  $\mathbf{T}_+$  and  $\mathbf{T}_-$ .  $\langle f | \mathbf{T}_\pm | g \rangle$  is then defined as the number of possible ways paths can move from the initial configuration encoded by  $f$  to the final configuration encoded by  $g$  in one time step according to the rules of evolution described in section 2.2, using only the  $2 \times 5$  tiles  $\alpha$  and  $\beta$  of Fig. 1. In principle one could assign weights to the different tiles but we shall not need to do so here. Note the relation  $\mathbf{T}_+ = \mathbf{S} \mathbf{T}_-$ . In the case of a two-row evolution, one can introduce  $\mathbf{T}^2 := \mathbf{T}_+ \mathbf{T}_- = \mathbf{T}_- \mathbf{T}_+$ , which has the advantage that it restores the left-right symmetry.<sup>1</sup>

Note that sufficiently far to the left, there are only green lines and these necessarily move one half-step to the left. On the contrary, far to the right, one has red lines that move one half-step to the right. This observation allows us to conclude that  $\mathbf{T}_\pm$  changes the charge by  $\mp 1$  and increases the emptiness number by 1, or equivalently  $\mathbf{T}^2$  preserves the charge, but increases the emptiness number by 2.

We now prove some additional properties of  $\mathbf{T}^2$ .

**Lemma 2.** *For any pair of basis states  $f$  and  $g$ ,*

$$\langle f | \mathbf{T}^2 | g \rangle \neq 0 \Rightarrow N_{-0}(f) \geq N_{-0}(g) + 1 \text{ and } N_{+0}(f) \leq N_{+0}(g) - 1$$

*Proof.* Since particles of the same color never cross, the leftmost or rightmost particles remain the same during time evolution. The lemma then follows from the fact that red (resp. green) particles move at least one half-step to the right (resp. left) at each time step. □

<sup>1</sup>Despite the notation,  $\mathbf{T}^2$  is not the square of an operator on  $\mathcal{G}$ ; if one insisted that it be so, one would have to define  $\mathbf{T}$  as acting on  $\mathcal{G} \oplus \mathcal{G}$ , with  $\mathbf{T} = \begin{pmatrix} 0 & \mathbf{T}_+ \\ \mathbf{T}_- & 0 \end{pmatrix}$ .

**Lemma 3.** *If  $|f\rangle = |f_-\rangle \sqcup |f_+\rangle \in \mathcal{G}_{\text{free}}$ , with  $N_+(f_-) \leq 0$  and  $N_-(f_+) \geq 0$ , then  $\mathbf{T}^2 |f\rangle \in \mathcal{G}_{\text{free}}$ , and*

$$\mathbf{T}^{2k} |f\rangle = |f_-\rangle \sqcup_k |f_+\rangle \quad \forall k \in \mathbb{Z}_+$$

*Proof.* Such a state  $|f\rangle$  has the properties that all green lines are to the left of red lines, so no crossings ever occur. Therefore, the green (resp. red) lines move one half-step to the left (resp. right) at each time step. This is all that the lemma says.  $\square$

**Lemma 4.** *Call  $p = \max(N_{+0}(f), -N_{-0}(f))$ . Then  $\mathbf{T}^{2p} |f\rangle \in \mathcal{G}_{\text{free}}$  and there exist unique coefficients  $c_{g,h}^f$  such that*

$$\mathbf{T}^{2k} |f\rangle = \sum_{g,h} c_{g,h}^f |g\rangle \sqcup_k |h\rangle \quad \forall k \geq p$$

Intuitively, this lemma says that no matter what the initial state is, eventually all possible crossings will take place and we shall be left with a linear combination of states which are all such that all green lines are to the left of red lines.

*Proof.* This is combination of the two preceding lemmas. Let  $|f\rangle$  be a basis state, and set  $p = \max(N_{+0}(f), -N_{-0}(f))$ . Then according to lemma 2,  $\mathbf{T}^{2p} |f\rangle$  is a linear combination of basis states  $|g\rangle$  such that  $N_{-0}(g) \geq 0$  and  $N_{+0}(g) \leq 0$ , i.e.  $\mathbf{T}^{2p} |f\rangle \in \mathcal{G}_{\text{free}}$ .

By definition of  $\mathcal{G}_{\text{free}}$ , this implies that there exist uniquely defined coefficients  $c_{g,h}^f$  such that  $\mathbf{T}^{2p} |f\rangle = \sum_{g,h} c_{g,h}^f |g\rangle \sqcup_p |h\rangle$ , where the summation is restricted to couples  $(g, h)$  such that  $N_+(g) < p$ ,  $N_-(h) > -p$ . Set all other entries  $c_{g,h}^f$  to zero. The formula of the lemma then follows by application of lemma 3.  $\square$

**Corollary.** *If  $|\lambda\rangle \in \mathcal{F} \subset \mathcal{G}$  is a state with zero charge and zero emptiness number and  $p = \max(N_+(f), -N_-(f))$ , then there exist unique coefficients  $c_{\mu,\nu}^\lambda$  such that*

$$\mathbf{T}^{2k} |\lambda\rangle = \sum_{\mu,\nu} c_{\mu,\nu}^\lambda |\mu\rangle \sqcup_k |\nu\rangle \quad \forall k \geq p$$

where the sum is over pairs of Young diagrams.

*Proof.* Such a state  $|\lambda\rangle$  has zero charge and zero emptiness number. The formula of lemma 3 implies that all pairs  $(g, h)$  that contribute to the sum satisfy  $0 = c(\lambda) = \frac{1}{2}(c(g) + c(h))$  and  $0 = e(\lambda) = \frac{1}{2}(c(g) - c(h))$ , so that they have zero charge themselves. They can therefore be indexed by Young diagrams.  $\square$

**4.3. The two families of commuting transfer matrices.** We define here two one-parameter families of transfer matrices  $\tilde{\mathbf{T}}_\pm(u)$ , which are closely connected to  $\mathbf{T}_\pm$ .

Naively, one would like to define  $\tilde{\mathbf{T}}_\pm$  as transfer matrices which, in addition to the usual tiles  $\alpha$  and  $\beta$ , allow one more type of tiles  $\gamma_\pm$ , but at a cost of a certain weight  $x$ . However, this turns out to be inconvenient for the boundary conditions we have in mind, so we use the following definition instead, using the inverse  $u = x^{-1}$  of the natural parameter  $x$  (which will reoccur in section 6).  $\tilde{\mathbf{T}}_\pm(u)$  is defined similarly as  $\mathbf{T}_\pm$ , but with three new ingredients: (i) we allow the extra tiles of type  $\gamma_\pm$  and (ii) we give a weight of  $u$  to each pair of tiles of

type  $\alpha_{\pm}$ , and to each pair of tiles of type  $\beta_{\pm}$  (all the signs being the same as that of the transfer matrix). (iii) we impose the following condition at infinity: sufficiently far to the left and to the right, the effect of  $\tilde{\mathbf{T}}_-(u)$  (resp.  $\tilde{\mathbf{T}}_+(u)$ ) must be to push either type of lines one half-step to the right (resp. left). Taking into account that this half-step is absorbed into the definition of the matrix, we find that at infinity  $\tilde{\mathbf{T}}_{\pm}(u)$  behaves like the identity. This ensures that only a finite number of tiles of type  $\alpha_{\pm}$  or  $\beta_{\pm}$  ever occur in the evolution w.r.t.  $\tilde{\mathbf{T}}_{\pm}(u)$ . Thus each entry of  $\tilde{\mathbf{T}}_{\pm}(u)$  is a polynomial in  $u$ .

The boundary conditions also imply that  $\tilde{\mathbf{T}}_{\pm}(u)$  preserves the charge and the emptiness number.

We now list some properties of  $\tilde{\mathbf{T}}_{\pm}(u)$ .

**Lemma 5.** *For any pair of basis states  $f$  and  $g$ ,*

$$\langle f | \tilde{\mathbf{T}}_+(u) | g \rangle \neq 0 \Rightarrow N_{-0}(f) \geq N_{-0}(g) - 1 \text{ and } N_{+0}(f) \leq N_{+0}(g)$$

$$\langle f | \tilde{\mathbf{T}}_-(u) | g \rangle \neq 0 \Rightarrow N_{-0}(f) \geq N_{-0}(g) \text{ and } N_{+0}(f) \leq N_{+0}(g) + 1$$

*Proof.* Same proof as lemma 2, but this time green particles can move one half-step to the right for  $\tilde{\mathbf{T}}_-$  and red particles can move one half-step to the left for  $\tilde{\mathbf{T}}_+$ .  $\square$

**Lemma 6.**  $|f\rangle = |f_-\rangle \sqcup |f_+\rangle \in \mathcal{G}_{\text{free}}$ , then

$$\begin{aligned} \tilde{\mathbf{T}}_-(u) |f\rangle &= \overline{\mathbf{T}}_{\text{free}}(u) |f_-\rangle \sqcup |f_+\rangle \\ \tilde{\mathbf{T}}_+(u) |f\rangle &= |f_-\rangle \sqcup \mathbf{T}_{\text{free}}(u) |f_+\rangle \end{aligned}$$

*Proof.* By inspection. If there are only green particles to the left of 0 and red particles to the right of 0, no crossings can occur. For  $\tilde{\mathbf{T}}_-(u)$ , this leaves two possibilities for green particles: going left one half-step (pair of tiles  $\alpha_-$ ) with a weight of  $u$  or going right one half-step (pair of tiles  $\gamma_-$ ) with a weight of 1; and only one possibility for red particles, going right one-half step (pair of tiles  $\alpha_+$ ) with a weight of 1. Adjusting the locations by shifting everything one half-step to the left, we obtain exactly  $\overline{\mathbf{T}}_{\text{free}}(u)$  for green particles and no evolution for red particles. The reasoning is the same for  $\tilde{\mathbf{T}}_+(u)$ .  $\square$

Note the similarity with lemma 3. However, an important difference with the situation of lemma 3 is that it is not true that  $|f\rangle \in \mathcal{G}_{\text{free}}$  implies  $\tilde{\mathbf{T}}_{\pm}(u) |f\rangle \in \mathcal{G}_{\text{free}}$ , so in general one cannot iterate the argument.

*Remark 3* (followup of *Remark 1*): intuitively, this means that when the sets of green and red particles are widely separated from each other then our transfer matrices make them evolve like free fermions. When green and red particles mix, it is not the case any more: in this sense what we have is a system of two species of fermions interacting with each other.

**Lemma 7.** *The transfer matrices  $\tilde{\mathbf{T}}_{\pm}(u)$  leave  $\mathcal{F} \subset \mathcal{G}$  stable, and:*

$$\begin{aligned} \tilde{\mathbf{T}}_-(u) |f\rangle &= \overline{\mathbf{T}}_{\text{free}}(u) |f\rangle & \forall |f\rangle \in \mathcal{F} \\ \tilde{\mathbf{T}}_+(u) |f\rangle &= \mathbf{T}_{\text{free}}(u) |f\rangle & \forall |f\rangle \in \mathcal{F} \end{aligned}$$

*Proof.*  $\mathcal{F}$  viewed as a subspace of  $\mathcal{G}$  is simply the subspace of zero emptiness number, and the  $\tilde{\mathbf{T}}_{\pm}(u)$  preserve this number, so they leave  $\mathcal{F}$  stable.

The rest of the reasoning is again by inspection. Consider the action of  $\tilde{\mathbf{T}}_+(u)$  on a state with no empty spots. Remembering that the final state should also have no empty spots (this is in fact a consequence of the boundary conditions, as already explained), we conclude that tiles of type  $\alpha_+$  are forbidden (consider the leftmost tile of type upper  $\alpha_+$ ; the only allowed tile left of it is the empty tile  $\beta_0$ ). Similarly tiles of type  $\beta_-$  are forbidden (sequences of such tiles always end with tiles of type  $\alpha_+$ ). All that we are left with is half-steps to the left (tiles  $\alpha_-$  and  $\gamma_+$ ) and crossings of the type  $\beta_+$ , that is one green line crossing a series of red lines. But up to an overall half-step to the left, these crossings are exactly those that occur between red and green lines in the free fermionic model, compare Figs. 3 and 5. The weight of  $u$  is given to each each pair of  $\beta_+$  tiles, that is to each crossing, which is the same weight that is given in the free fermionic model.

A similar reasoning works for  $\tilde{\mathbf{T}}_-(u)$  and  $\overline{\mathbf{T}}_{\text{free}}(u)$ .  $\square$

**Theorem 1.** All transfer matrices  $\tilde{\mathbf{T}}_-(u)$ ,  $\tilde{\mathbf{T}}_+(v)$ ,  $\mathbf{T}$  commute:

$$[\tilde{\mathbf{T}}_\epsilon(u), \tilde{\mathbf{T}}_{\epsilon'}(v)] = 0 \quad [\tilde{\mathbf{T}}_\epsilon(u), \mathbf{T}_{\epsilon'}] = 0 \quad \epsilon, \epsilon' \in \{+, -\}$$

This is the central result, embodying the integrability of the model. Its proof is the subject of section 6.

## 5. LITTLEWOOD–RICHARDSON COEFFICIENTS

### 5.1. The coproduct formula.

**Theorem 2.** The coefficients  $c_{\mu, \nu}^\lambda$  in the corollary of lemma 4 are Littlewood–Richardson coefficients.

*Proof.* Start from the supersymmetric Schur function (lemma 1)

$$s_\lambda(u_1, \dots, u_m/v_1, \dots, v_n) = \langle \emptyset | \prod_{i=1}^m \mathbf{T}_{\text{free}}(u_i) \prod_{i=1}^n \overline{\mathbf{T}}_{\text{free}}(v_i) | \lambda \rangle$$

Considering  $|\emptyset\rangle$  and  $|\lambda\rangle$  as states in  $\mathcal{G}$ , we immediately find by applying lemma 7:

$$s_\lambda(u_1, \dots, u_m/v_1, \dots, v_n) = \langle \emptyset | \prod_{i=1}^m \tilde{\mathbf{T}}_+(u_i) \prod_{i=1}^n \tilde{\mathbf{T}}_-(v_i) | \lambda \rangle$$

Given a non-negative integer  $k$ , consider the evolution *backwards in time* (i.e. going downwards instead of upwards) starting from  $\langle \emptyset | \sqcup_k \langle \emptyset |$ . It is elementary to check that after  $2k$  steps, one gets  $\langle \emptyset |$ , or in other words  $\langle \emptyset | = \langle \emptyset | \sqcup_k \langle \emptyset | \mathbf{T}^{2k}$ . This results in

$$s_\lambda(u_1, \dots, u_m/v_1, \dots, v_n) = \langle \emptyset | \sqcup_k \langle \emptyset | \mathbf{T}^{2k} \prod_{i=1}^m \tilde{\mathbf{T}}_+(u_i) \prod_{i=1}^n \tilde{\mathbf{T}}_-(v_i) | \lambda \rangle$$

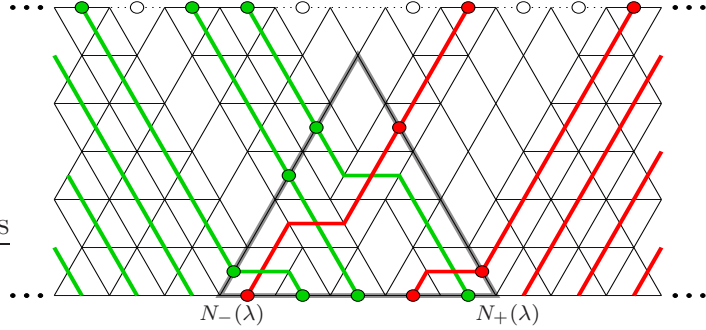


FIGURE 6. An example of configuration and the triangle in which all the crossings take place.

We now use the commutation of the transfer matrices (theorem 1) to rewrite it

$$s_\lambda(u_1, \dots, u_m/v_1, \dots, v_n) = \langle \emptyset | \sqcup_k \langle \emptyset | \prod_{i=1}^m \tilde{\mathbf{T}}_+(u_i) \prod_{i=1}^n \tilde{\mathbf{T}}_-(v_i) \mathbf{T}^{2k} | \lambda \rangle$$

Assume  $k > \max(N_+(\lambda), -N_-(\lambda))$ , and apply the corollary of lemma 4:

$$s_\lambda(u_1, \dots, u_m/v_1, \dots, v_n) = \sum_{\mu, \nu} c_{\mu, \nu}^\lambda \langle \emptyset | \sqcup_k \langle \emptyset | \prod_{i=1}^m \tilde{\mathbf{T}}_+(u_i) \prod_{i=1}^n \tilde{\mathbf{T}}_-(v_i) | \mu \rangle \sqcup_k | \nu \rangle$$

We now wish to apply lemma 6.  $|\mu\rangle \sqcup_k |\nu\rangle \in \mathcal{G}_{\text{free}}$ , but as already mentioned  $\tilde{\mathbf{T}}_+(u)$  may push red particles to the left and  $\tilde{\mathbf{T}}_-(u)$  may push green particles to the right. Let us thus choose  $k > \max(N_+(\lambda), -N_-(\lambda)) + n/2$ ; according to lemma 5, this ensures that lemma 6 can be applied repeatedly. Separating into two bra-kets, we get:

$$s_\lambda(u_1, \dots, u_m/v_1, \dots, v_n) = \sum_{\mu, \nu} c_{\mu, \nu}^\lambda \langle \emptyset | \prod_{i=1}^m \mathbf{T}_{\text{free}}(u_i) | \nu \rangle \langle \emptyset | \prod_{i=1}^n \overline{\mathbf{T}}_{\text{free}}(v_i) | \mu \rangle$$

Finally, apply the basic free fermionic identity (lemma 1): we find

$$s_\lambda(u_1, \dots, u_m/v_1, \dots, v_n) = \sum_{\mu, \nu} c_{\mu, \nu}^\lambda s_\nu(u_1, \dots, u_m) s_{\mu^T}(v_1, \dots, v_n)$$

Remembering that the l.h.s. is the supersymmetric Schur function associated to  $\lambda$ , we conclude that this equality defines uniquely the  $c_{\mu, \nu}^\lambda$  as Littlewood-Richardson coefficients.  $\square$

**5.2. Back to the triangle.** All that has been described so far uses an infinite-dimensional Fock space of configurations. This helps in formulating the results more elegantly. However, for any given Young diagram  $\lambda$ , all the evolution of the state  $|\lambda\rangle$  with respect to  $\mathbf{T}$  takes place in a finite part of the plane; more precisely, a triangle, which leads us back to the more standard formulation, as in [10], in terms of puzzles.

First, let us define how to read Young diagrams from the boundaries of a finite domain (this is a finitized version of the transformation of section 3.1). Let  $n$  and  $k$  be two non-negative integers such that  $k \leq n$ . Consider a sequence of  $n$  successive edges which can be either  $-$  or  $+$ , such that there are  $k$   $-$  and  $n - k$   $+$ . Fix an orientation of the edge: then reading the values of the edges following the orientation, one obtains a binary string

of length  $n$ . To it one associates bijectively a Young diagram contained inside the Young diagram  $k \times (n - k)$ , that is the rectangle of height  $k$  and width  $n - k$ , as follows: each  $-$  corresponds to a step up, and each  $+$  to a step to the right, starting from the lower left corner of the rectangle. For example,

$$+ - + + - + \mapsto \begin{array}{c} \text{Young diagram} \\ \equiv \end{array} \begin{array}{c} \text{Young diagram} \end{array}$$

Note that depending on the direction of the boundary, a  $-$  will be drawn as a green particle or an empty spot, and a  $+$  will be drawn as a red particle or an empty spot.

Let us now fix an initial state given by a Young diagram  $\lambda$  and consider the possible evolution of the system. The situation is illustrated on Fig. 6. The smallest possible triangle in which all crossings between green and red particles take place has as its lower side the interval between  $N_-(\lambda)$  and  $N_+(\lambda)$ . So we can set  $n = N_+(\lambda) - N_-(\lambda)$ , in which case  $k$  is the height of  $\lambda$  (number of non-zero parts). Of course one could make the triangle bigger, which illustrates the stability property of puzzles. Now the configuration outside the triangle is uniquely fixed by the locations of the lines at the two upper sides of the triangle: green (resp. red) particles move uniformly to the left (resp. right). In other words, no information is lost by restricting to the triangle and conversely, any configuration inside the triangle can be extended to the outside in a unique way. The “asymptotic” states  $\mu$  and  $\nu$  which describe the sequences of green particles and empty spots to the left and of red particles and empty spots to the right can also be read off the two upper sides of the triangle in the way described in the previous paragraph, the binary strings being read from left to right. Combining these observations, we conclude that  $c_{\mu, \nu}^\lambda$  also counts the number of fillings of the triangle with fixed boundaries, where  $\lambda$  is encoded by the bottom edge,  $\mu$  by the left edge and  $\nu$  by the right edge, always reading from left to right. These fillings are called *puzzles*. For example, on Fig. 6, one reads

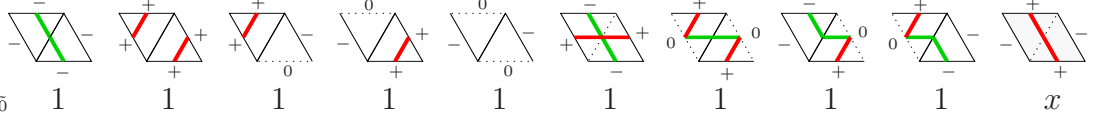
$$\lambda = \begin{array}{c} \text{Young diagram} \end{array}, \quad \mu = \nu = \begin{array}{c} \text{Young diagram} \end{array}.$$

## 6. PROOF OF THE COMMUTATION THEOREM

We now provide the proof of theorem 1.

**6.1.  $R$ -matrix and Yang–Baxter equation.** The first idea is to decompose the action of the transfer matrices as products of elementary blocks, called  $R$ -matrices. It is convenient in this section to go back to the labels  $+, -, 0, \tilde{0}$  on the edges because using it, the tiles are explicitly  $\mathbb{Z}_3$ -invariant. We can then choose as elementary blocks two adjacent triangles. They have three possible orientations, which correspond to three possible rhombi.

Let us choose for example the orientation as shown on Fig. 7, and allow the tiles  $\alpha_\pm, \beta_{\pm 0}, \gamma_+$ , with the weights indicated below.  $x$  is the *spectral parameter*. In fact the only rule is that pairs of shaded tiles get a weight of  $x$ . The weights look different but are actually equivalent to the weights of  $\tilde{\mathbf{T}}_+(v)$ , with  $v = 1/x$  (this will be explained in the next section). The colored lines are only decorative here and the focus is on the edge numbers. We can encode

FIGURE 7. The  $R$ -matrix in one of its three orientations.

this information into a  $3 \times 3 \times 3 \times 3$  tensor as follows.  $\mathbf{R}_{i,j,k,l}(x)$ , where each index lives in  $\{-, +, 0\}$ , is the weight of the rhombus with edges  $i, j, k, l$  read counterclockwise starting from the left edge (or the right edge, the tiles being 180 degrees symmetric).

$\mathbf{R}(x)$  is usually considered as a matrix by associating to it the map from  $\mathbb{C}^3 \otimes \mathbb{C}^3$  (corresponding to the left and bottom edges) to itself (corresponding to the right and top edges); explicitly,

$$(6.1) \quad \mathbf{R}(x) = \begin{pmatrix} -,- & -,+ & -,0 & +,- & +,+ & +,0 & 0,- & 0,+ & 0,0 \\ -,- & \begin{pmatrix} 1 & 0 & 0 & 0 & 0 & 0 & 0 & 0 & 0 \\ 0 & x & 0 & 0 & 0 & 1 & 1 & 0 & 0 \\ 0 & 0 & 1 & 0 & 0 & 0 & 0 & 0 & 0 \\ 0 & 0 & 0 & 1 & 0 & 0 & 0 & 0 & 0 \\ 0 & 0 & 0 & 0 & 1 & 0 & 0 & 0 & 0 \\ 0 & 1 & 0 & 0 & 0 & 0 & 0 & 0 & 0 \\ 0 & 1 & 0 & 0 & 0 & 0 & 0 & 0 & 0 \\ 0 & 0 & 0 & 0 & 0 & 0 & 0 & 1 & 0 \\ 0 & 0 & 0 & 0 & 0 & 0 & 0 & 0 & 0 \end{pmatrix} \\ -,+ & \dots \\ -,0 & \dots \\ +,- & \dots \\ +,+ & \dots \\ +,0 & \dots \\ 0,- & \dots \\ 0,+ & \dots \\ 0,0 & \dots \end{pmatrix}$$

This point of view is not particularly useful for our purposes because it breaks the  $\mathbb{Z}_3$  rotational symmetry by forcing to distinguish “incoming” and “outgoing” edges.

Rotate now every tile 120 degrees clockwise: we obtain the tiles  $\alpha_{\pm}$ ,  $\beta_{\pm 0}$ ,  $\gamma_-$  (which are exactly the tiles of  $\tilde{\mathbf{T}}_-(v)$ ). This time it is  $\gamma_-$  pairs (again, the shaded tiles) which get a weight of  $x$ . Finally, there exists a third possible orientation of rhombi, obtained from the first set of tiles by 120 degrees counterclockwise rotation – and correspondingly, a third shaded tile which has not been used so far, namely  $\gamma_0$ . We shall use the following graphical notation for these three types of  $R$ -matrices: simply depict them with rhombi (with thick edges) and put the spectral parameter  $x$  inside. The convention is that when several rhombi are pasted together, the internal edges are free i.e. summed over while the external edges are fixed.

We now have the key proposition, which is the Yang–Baxter equation:

**Proposition 1.** *Let three variables  $x, y, z$  satisfy  $x+y+z=0$ . Then, the following equality holds*

for any values of the external edges while summing over the matching tiles inside.

*Proof.* The proof is just an explicit computation. We provide a particularly compact version of it, which was suggested to the author by A. Knutson.

Note first that if the equation is true for a given sequence of external edges, then it is true for any cyclic rotation of it: indeed a rotation of 120 degrees amounts to cyclic permutation of the variables, and a rotation of 180 degrees amounts to exchanging l.h.s. and r.h.s. (the tile weights being invariant by 180 degrees rotation).

Next, observe that if no shaded tiles appear in the equality, then it is trivial – the different types of rhombi are only distinguished by the additional shaded tiles which carry a non-trivial weight. If there are such pieces, then necessarily one of the external sides of the tiles must be a sequence of  $-$ ,  $+$  (read counterclockwise). This leaves only three possible sequences of external edges, up to cyclic rotation: (i)  $-$ ,  $+$ ,  $-$ ,  $-$ ,  $+$ ,  $-$ , (ii)  $-$ ,  $+$ ,  $+$ ,  $-$ ,  $+$ ,  $+$  and (iii)  $-$ ,  $+$ ,  $-$ ,  $+$ ,  $-$ ,  $+$ . The first two sequences are invariant by 180 degrees, which allows to prove the equality without calculation, since as already mentioned the 180 degrees rotation of the l.h.s. is the r.h.s. The last case is the only interesting one: we find the identity

(or its 180 degrees rotation), that is  $x + y + z = 0$ .  $\square$

**6.2. The RTT relations.** We use the notation  $\mathbf{T}_\pm^{a,b}(x)$  for the transfer matrix that creates one extra row made of the usual tiles  $\alpha$ ,  $\beta$  and  $\gamma_\pm$ , followed as usual by a  $\pm\frac{1}{2}$ -step, in such a way that sufficiently far to the left the left sides of the rhombi are all  $a$  and sufficiently far to the right the right sides of the rhombi are all  $b$ . The weights are those of  $\mathbf{R}$ , divided by a factor  $\kappa_\pm^{a,b}$  if say the value of the upper edge is equal to  $\pm$ , which makes sure that the tiles have weight 1 sufficiently far to the left and right. Explicitly,  $\kappa_+^{a,b} = \mathbf{R}_{a,+a,+}$  and  $\kappa_-^{a,b} = \mathbf{R}_{-,b,-b}$ . In practice we shall only consider here the cases  $\mathbf{T}_\pm^{-,+}$ ,  $\mathbf{T}_+^{-,-}$  and  $\mathbf{T}_-^{+,+}$ , in which case we recover.

$$\mathbf{T}_\pm = \mathbf{T}_\pm^{-,+}(0) \quad \tilde{\mathbf{T}}_+(u) = \mathbf{T}_+^{-,-}(u^{-1}) \quad \tilde{\mathbf{T}}_-(u) = \mathbf{T}_-^{+,+}(u^{-1})$$

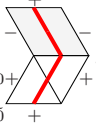
We now apply the standard argument of repeated application of the Yang–Baxter equation (“unzipping”) to write the RTT relations, which allow to show various commutation relations.

Let us fix two basis elements  $|f\rangle$  and  $|g\rangle$  in  $\mathcal{G}$  and consider matrix elements of the form  $\langle f | \mathbf{T}_+^{a,b}(x) \mathbf{T}_-^{c,d}(y) | g \rangle$ . The important observation is that to the left of  $\min(N_-(f), N_-(g))$ , one has series of identical tiles. Thus no information is lost by truncating the state anywhere left of  $\min(N_-(f), N_-(g))$ , and the product of weights of the discarded left tiles is 1. Similarly, to the right of  $\max(N_+(f), N_+(g))$ , everything is frozen and we only have weights of 1.

Note that we already know this to be the case “sufficiently far to the left”, but this is not good enough for our purposes: we need a bound that is uniform w.r.t. the intermediate state. For example if  $a = b = -$  and  $c = d = +$ , one can check that the infinite sequence

of on the left side and of on the right side can only stop when the upper or lower edges change their value.

In the case  $a = b = -$  and  $c = -, d = +$ , there is no change to the right of  $\max(N_+(f), N_+(g))$ ,

where we find again sequences of . However, to the left of  $\min(N_-(f), N_-(g))$ , we have

a new situation where green lines move one full step to the left, that is sequences of .

The two other cases of interest to us can be treated similarly.

Thus, if we pick any region containing the interval  $[\min(N_-(f), N_-(g)), \max(N_+(f), N_+(g))]$ , we can write that

$$(\kappa_+^{a,b})^r (\kappa_-^{c,d})^g \langle f | \mathbf{T}_+^{a,b}(x) \mathbf{T}_-^{c,d}(y) | g \rangle = \begin{array}{c} f \\ \hbox{\scriptsize hexagonal tiling} \\ g \end{array}$$

where the tiling consists of hexagons with labels  $x$  and  $y$  on the horizontal edges, and  $a, b, c, d$  on the vertical edges. The boundary is indicated by a dashed line.

where  $g$  (resp.  $r$ ) denotes the number of green (resp. red) lines in the finite domain, which is well-defined if  $b = -$  (resp.  $c = +$ ) because no green (resp. red) line can cross the boundary with such boundary conditions (and these are the only cases where the factors  $\kappa$  are not 1).

At this stage, we can insert the  $R$ -matrix at the left, with spectral parameter  $z = -x - y$ :

$$\sum_{a,c} \mathbf{R}_{c',a',c,a}(z) (\kappa_+^{a,b})^g (\kappa_-^{c,d})^r \langle f | \mathbf{T}_+^{a,b}(x) \mathbf{T}_-^{c,d}(y) | g \rangle = \begin{array}{c} f \\ \hbox{\scriptsize hexagonal tiling} \\ g \end{array}$$

where the tiling consists of hexagons with labels  $x$  and  $y$  on the horizontal edges, and  $a, b, c, d$  on the vertical edges. The boundary is indicated by a dashed line.

We apply repeatedly proposition 1 all the way to

$$\begin{aligned} \sum_{a,c} \mathbf{R}_{c',a',c,a}(z) (\kappa_+^{a,b})^g (\kappa_-^{c,d})^r \langle f | \mathbf{T}_+^{a,b}(x) \mathbf{T}_-^{c,d}(y) | g \rangle &= \begin{array}{c} f \\ \hbox{\scriptsize hexagonal tiling} \\ g \end{array} \\ &= \sum_{b',d'} \mathbf{R}_{d',b',d,b}(-x - y) (\kappa_+^{a',b'})^r (\kappa_-^{c',d'})^g \langle f | \mathbf{T}_-^{c',d'}(y) \mathbf{T}_+^{a',b'}(x) | g \rangle \end{aligned}$$

By varying  $a', b, c', d$  one gets in principle 81 identities relating transfer matrices with various boundary conditions. We are only interested in the four cases  $a' = -, b \in \{+, -\}$ ,  $c' \in \{+, -\}$ ,  $d = +$  which lead to the following

**Theorem 3.** *We have the commutation relations*

$$[\mathbf{T}_+^{-,-}(x), \mathbf{T}_-^{-,+}(y)] = [\mathbf{T}_+^{-,-}(x), \mathbf{T}_-^{+,+}(y)] = [\mathbf{T}_+^{-,+}(x), \mathbf{T}_-^{-,+}(y)] = [\mathbf{T}_+^{-,+}(x), \mathbf{T}_-^{+,-}(y)] = 0$$

This theorem implies that  $[\tilde{\mathbf{T}}_+(u), \tilde{\mathbf{T}}_-(v)] = 0$ , as well as  $[\tilde{\mathbf{T}}_\epsilon(u), \mathbf{T}_{\epsilon'}] = 0$ ,  $\epsilon, \epsilon' \in \{-, +\}$ .

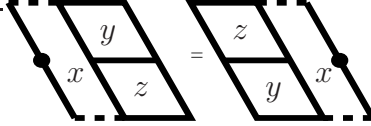


FIGURE 8. Graphical representation of the Yang–Baxter equation with one matrix  $\mathbf{R}^*(x)$  and two matrices  $\mathbf{R}(y)$ ,  $\mathbf{R}(z)$ . Here  $x = z - y$ .

**6.3. Other cases.** In order to complete the proof of theorem 1, we must show the commutation  $[\tilde{\mathbf{T}}_\pm(u), \tilde{\mathbf{T}}_\pm(v)] = 0$  (same sign). This requires another kind of  $R$ -matrix, as the geometry suggests, cf Fig. 8. We do not provide the details since these commutation relations are not needed anywhere. Let us simply give the expression of the new  $R$ -matrix:

$$\mathbf{R}^*(x) = \begin{pmatrix} -, - & -, + & -, 0 & +, - & +, + & +, 0 & 0, - & 0, + & 0, 0 \\ -,- & \begin{pmatrix} 1 & 0 & 0 & 0 & 0 & 0 & 0 & 0 & 0 \\ 0 & x & 0 & 1 & 0 & 0 & 0 & 0 & 0 \\ 0 & 0 & x & 0 & 0 & 0 & 1 & 0 & 0 \\ 0 & 1 & 0 & 0 & 0 & 0 & 0 & 0 & 0 \\ 0 & 0 & 0 & 0 & 1 & 0 & 0 & 0 & 0 \\ 0 & 0 & 0 & 0 & 0 & 0 & 0 & 1 & 0 \\ 0 & 0 & 1 & 0 & 0 & 0 & 0 & 0 & 0 \\ 0 & 0 & 0 & 0 & 0 & 1 & 0 & x & 0 \\ 0 & 0 & 0 & 0 & 0 & 0 & 0 & 0 & 1 \end{pmatrix} \end{pmatrix}$$

The rest of the proof is identical (unzipping argument) and we obtain the following

**Theorem 4.** *We have the commutation relations*

$$[\mathbf{T}_+^{-,-}(x), \mathbf{T}_+^{-,-}(y)] = [\mathbf{T}_-^{+,+}(x), \mathbf{T}_-^{+,+}(y)] = [\mathbf{T}_+^{-,+}(x), \mathbf{T}_+^{-,+}(y)] = [\mathbf{T}_-^{-,+}(x), \mathbf{T}_-^{-,+}(y)] = 0$$

Note that this theorem does *not* say that  $\mathbf{T}_+^{-,-}$  and  $\mathbf{T}_+^{-,+}$  commute.

## 7. EQUIVARIANCE OR THE INTRODUCTION OF INHOMOGENEITIES

It is natural to try to generalize the construction of section 5 by putting arbitrary horizontal and vertical spectral parameters (inhomogeneities) at each site. As already observed in [4, 12, 3] in a different but similar setting, this amounts geometrically to going from ordinary cohomology to equivariant cohomology – in the present case, of the Graßmannian.

There are however some complications. The first one is that the functions that naturally appear in this framework, factorial (or double) Schur functions, have more limited stability properties than simple Schur functions, and therefore the infinite system viewpoint used so far, whose whole purpose was to display these properties, is not particularly convenient. We shall therefore work in a finite domain instead.

The second one is that the coproduct formula does not obviously generalize to the inhomogeneous case. In fact, a coproduct formula for double Schur functions has only recently been discovered [14] and the description in terms of objects analogous to puzzles is unknown. We shall prove instead product formulae. Note that even specialized to the non-equivariant case, the formulae of this section will thus be distinct from those of section 5.

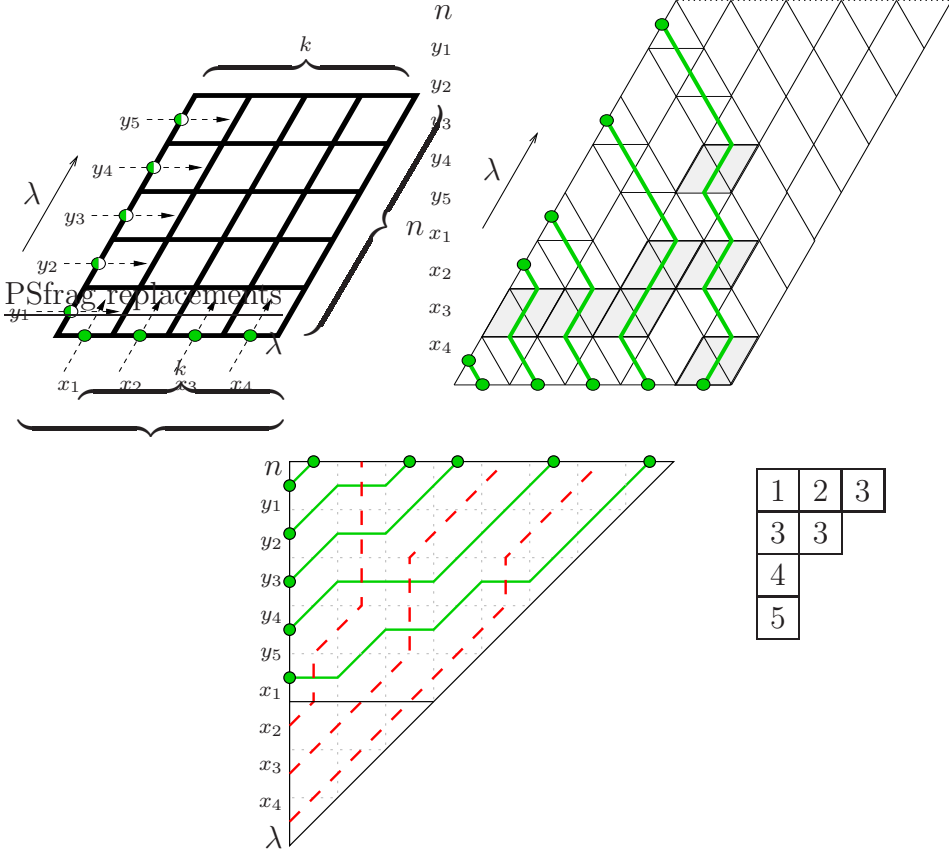


FIGURE 9. Our definition of factorial Schur functions, and an example in various graphical representations. The numbering of the  $x_i$  is reversed in the tableau representation.

The basis setup is to consider that there are (oriented) lines of spectral parameters propagating on the *dual lattice* of the lattice of tiles of  $R$ -matrices, in such a way that the spectral parameter attached to the tile is the difference of the two spectral parameters crossing it:

$$\begin{array}{ccc}
 & y & \\
 & \nearrow & \\
 \begin{array}{c} \text{---} \\ \text{---} \\ \text{---} \end{array} & z & = \quad \begin{array}{c} \text{---} \\ \text{---} \\ \text{---} \end{array} & y - z
 \end{array}$$

In all that follow we fix integers  $n$  and  $k$ ,  $k \leq n$ , and use the same correspondence between binaray strings and Young diagrams inside the rectangle  $k \times (n - k)$  described in section 5.2.

We now define the two basic “building blocks” with which we shall produce non-trivial identities.

**7.1. Factorial Schur functions.** What we really want to define is the double Schubert polynomial of a Graßmannian permutation. It will however coincide with the notion of factorial Schur function.

Given a Young diagram  $\lambda$  inside the rectangle  $k \times (n - k)$ , let us define the factorial Schur function  $s_\lambda(x_1, \dots, x_k | y_1, \dots, y_n)$  graphically as on Fig. 9, that is as a tiling of a  $n \times k$  rhombus with prescribed boundaries:  $\lambda$  is encoded into the edges of the left side, read from bottom to top, the bottom side is full of green particles and the other two sides are empty (in all the figures of this section, we omit entirely drawing empty spots, and use half-colored circles to indicate that the spot can be either empty or occupied by a particle of the given color, depending on the Young diagram it encodes). The spectral parameters are the  $x_i$  and the  $y_i$ , from left to right and bottom to top.

An important property is the following:

**Proposition 2.**  $s_\lambda(x_1, \dots, x_k | y_1, \dots, y_n)$  is a symmetric function of the  $x_i$ ,  $i = 1, \dots, k$ .

*Proof.* Fix  $i \in \{1, \dots, n - 1\}$  and apply the matrix  $\mathbf{R}^*(x_{i+1} - x_i)$  from section 6.3 to the bottom edges  $i$  and  $i+1$ . Noting that  $\mathbf{R}_{i,j,-,-}^* = \delta_{i,-}\delta_{j,-}$  and  $\mathbf{R}_{i,j,0,0}^* = \delta_{i,0}\delta_{j,0}$ , we can use the usual unzipping argument (repeated application of the Yang–Baxter relation represented on Fig. 8) to move the matrix  $\mathbf{R}^*(x_{i+1} - x_i)$  all the way to the top and then remove it. The result is the same picture as we started from, but with  $x_i$  and  $x_{i+1}$  exchanged.  $\square$

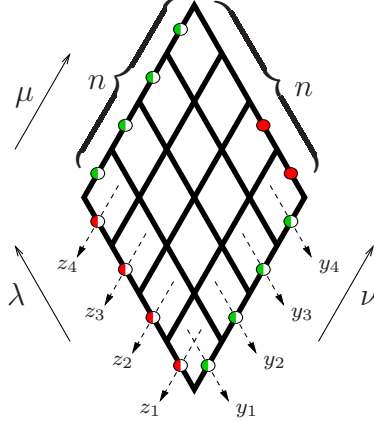
On Fig. 9, an example of configuration is provided, as well as two alternative representations of it. The first one is the *pipe dream* of the Graßmannian permutation associated to  $\lambda$  [5, 9]. Our picture can be deformed into the pipe dream picture by rotating 60 degrees clockwise and then distorting it slightly to make the 60 degrees angle a right angle. This way, the green lines are exactly the trajectories of the lines above the descent of the permutation. The other lines can be recovered unambiguously. The weights are now given to the crossings (between a red line and a green line) and take the form  $x_i - y_j$ , where  $i$  is the row number and  $j$  the column number, both counted starting from the corner.

The final representation is a semi-standard Young tableau of  $\lambda$ , with the alphabet  $\{1, \dots, k\}$ . Starting from the pipe dream picture, each column of the tableau corresponds to a red line counted from left to right, and each number in the boxes of the column indicates the row at which the red line crosses a green line. An important difference is that the rows are numbered from bottom to top; but since the factorial Schur function is a symmetric function of the  $x_i$ , this is irrelevant, and we may as well assign to the tableau a weight equal to the product over boxes of  $x_T - y_{T+c}$ , where  $T$  is the number in the box (i.e. the row number in the pipe dream picture) and  $c$  is the content of the box (column minus row of the box), in such a way that  $T + c$  is precisely the column number in the pipe dream picture.

**7.2. MS-puzzles and equivariant puzzles.** We first define an MS-puzzle (this terminology is borrowed from [10]). It is simply given by Fig. 10. Three sides encode Young diagrams, whereas the fourth side, the upper right one, is simply a sequence of  $+^{n-k} -^k$ , all read from bottom to top. We denote this object by  $e_{\lambda,\mu}^\nu(y_1, \dots, y_n; z_1, \dots, z_n)$ .

We shall need the following series of lemmas:

**Lemma 8.** *In the top half of a MS-puzzle, green lines always go in straight lines (up and to the left).*

FIGURE 10. Definition of an MS-puzzle ( $k = 2, n = 4$ ).

*Proof.* By inspection. Since the red lines are stacked at their rightmost positions, there is no available free spot for a green particle to cross the red particles by moving straight to the right.  $\square$

**Lemma 9.** *Assume that  $z_{n+1-i} = y_i$ ,  $i = 1, \dots, n$ . Then the top half of the MS-puzzle is “frozen” i.e. it has a unique configuration (which has weight 1); the edges on the horizontal diagonal of the MS-puzzle reproduce, read from left to right, the Young diagram  $\mu$ .*

*Proof.* If  $z_{n+1-i} = y_i$  for all  $i$ , then the rhombi sitting on the horizontal diagonal of the MS-puzzle have a zero spectral parameter. This implies that the shaded tiles  $\gamma_0$  is forbidden, or equivalently that the edges crossing horizontally these rhombi cannot be  $\bar{0}$  (red and green particles on top of each other). Since there are  $k$  green and  $n - k$  red lines incoming, there cannot be an empty spot either (edge 0). So these edges can only be  $+$  or  $-$ ; according to lemma 8, the green particles on it are at the same locations as on the upper left edge, and therefore the red lines are also fixed (they must move one step to the left each time they cross a green line) and occupy the complementary set on the diagonal. In other words, the diagram  $\mu$  is reproduced on the diagonal. No shaded tiles are used in the top half, so its weight is one.  $\square$

With the hypothesis of the last lemma, the top half of the MS-puzzle can be removed since it is fixed and has a weight of 1. The result, after 180 degree rotation, is called an *equivariant puzzle*, cf Fig. 11.

If we call  $c_{\mu, \lambda}^\nu$  the weight of an equivariant puzzle, that is the tiling of a triangle with sides  $\nu$  (bottom),  $\mu$  (left),  $\lambda$  (right), all read from left to right, with the same tiles and spectral parameters as an upside-down MS-puzzle with  $z_{n+1-i} = y_i$ , we have

$$e_{\lambda, \mu}^\nu(z_n, \dots, z_1; z_1, \dots, z_n) = c_{\bar{\nu}, \lambda}^{\bar{\mu}}(z_1, \dots, z_n)$$

or equivalently  $c_{\mu, \lambda}^\nu(z_1, \dots, z_n) = e_{\lambda, \bar{\nu}}^{\bar{\mu}}(z_n, \dots, z_1; z_1, \dots, z_n)$ , where  $\bar{\lambda}$  is the complement of the Young diagram  $\lambda$  inside the rectangle  $k \times (n - k)$  after a 180 degree rotation, which corresponds to reading the binary string of  $\lambda$  from right to left.

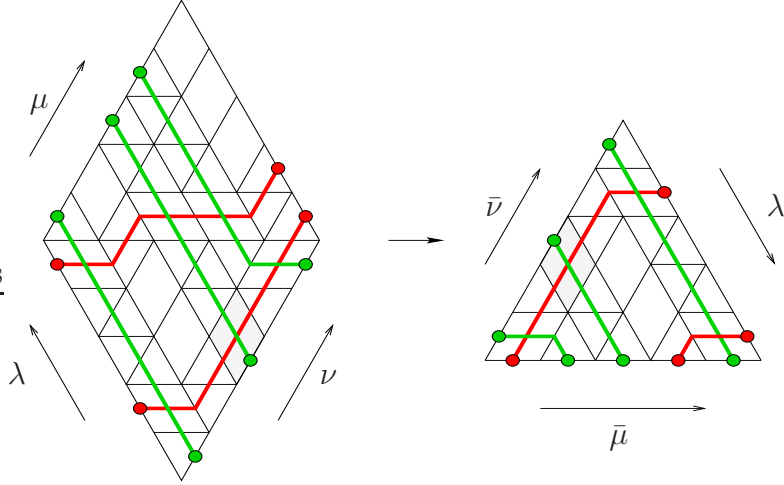


FIGURE 11. From an MS-puzzle to an equivariant puzzle.

**Lemma 10.** *There are no equivariant puzzles contributing to  $c_{\emptyset, \mu}^\nu$  or  $c_{\mu, \emptyset}^\nu$  if  $\mu \neq \nu$ , and one (which has no shaded tiles) if  $\mu = \nu$ , so that:*

$$c_{\emptyset, \mu}^\nu(z_1, \dots, z_n) = c_{\mu, \emptyset}^\nu(z_1, \dots, z_n) = \delta_\mu^\nu$$

*Proof.* Considering the equivariant puzzle as the bottom piece of an MS-puzzle, apply lemma 9 to either the mirror image w.r.t. the horizontal axis of the MS-puzzle with colors interchanged, or its 180 degree rotation.  $\square$

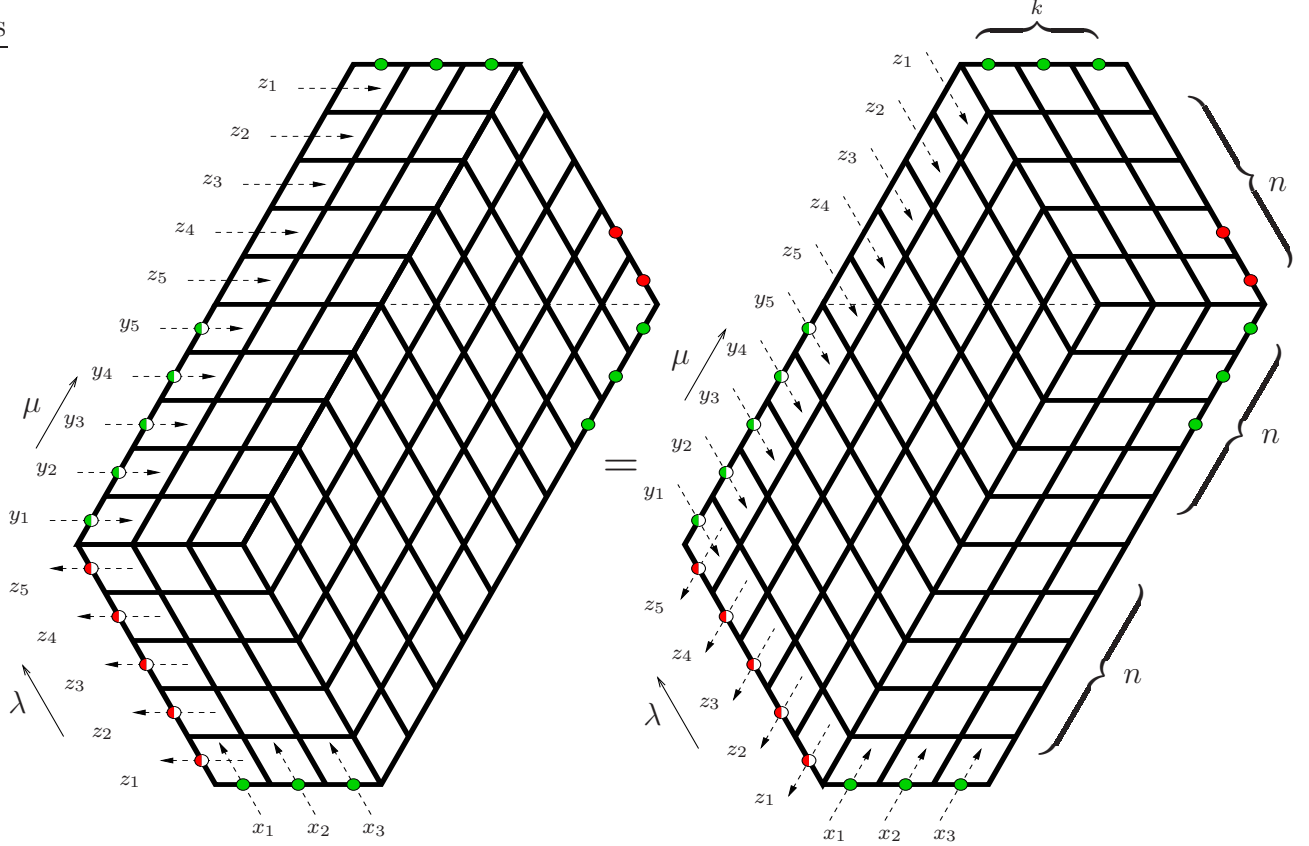
Finally, note that if all spectral parameters are equal to zero, we find by definition  $c_{\lambda, \mu}^\nu(0, \dots, 0) = c_{\lambda, \mu}^\nu$ ; which implies  $e_{\lambda, \mu}^\nu(0, \dots, 0; 0, \dots, 0) = c_{\nu, \lambda}^\mu$ . Rotating a (non-equivariant) puzzle 60 degrees counterclockwise results in another puzzle, so that  $c_{\nu, \lambda}^\mu = c_{\lambda, \mu}^\nu$ . To summarize,

$$c_{\lambda, \mu}^\nu(0, \dots, 0) = e_{\lambda, \mu}^\nu(0, \dots, 0; 0, \dots, 0) = c_{\lambda, \mu}^\nu$$

**7.3. The Molev–Sagan problem.** The Molev–Sagan (MS) problem consists in expanding the product of two factorial Schur functions with the same *first* set of variables as a sum of factorial Schur functions. It was first solved in [15] in terms of barred tableaux and then reformulated in [10] in terms of MS-puzzles. We now rederive it in our framework.

Let us consider the formal equality of Fig. 12. On each side of the equality, we have configurations where all the external edges are fixed. The order of the parameters  $y_i$  and  $z_i$  is important; note in particular the dashed line which corresponds to the difference of spectral parameters vanishing.

On the upper left side, we have a Young diagram  $\mu$  encoded by a binary string of green particles and empty spots in the region of parameters  $y_i$ , and emptiness above in the region of the  $z_i$ . On the lower left side, we have a Young diagram  $\lambda$  encoded by a binary string of green particles and empty spots. Both diagrams are read from bottom to top. The right sides have  $k$  green particles at their highest possible location and  $n - k$  red particles at their lowest possible location. The top and bottom sides are full of green particles. Furthermore,

FIGURE 12. Graphical solution of the MS problem ( $n = 5, k = 3$ ).

we assume that the sum of widths  $\mu_1 + \lambda_1$  of the Young diagrams  $\mu$  and  $\lambda$  does not exceed  $n - k$ . This can always be achieved by choosing  $n$  sufficiently large. The justification of this assumption will become clear below.

In order to go from one side to the other side of the figure, one simply applies repeatedly proposition 1 (Yang–Baxter) starting from the center and “piling up boxes”. Since our spectral parameters are differences of the parameters of crossing lines, the sum of spectral parameters around a hexagon is indeed zero.

We shall now examine what the consequences of this equality are. It is simpler to work on an example, as on Fig. 13. For ease of discussion, we have labelled the various regions inside the hexagon and marked in blue the “interesting” ones, that is those in which there is some freedom left – the other regions are entirely “frozen” once the boundary conditions are fixed.

Let us start with the left hand side. In region A, green particles starting from the bottom can only go straight to the left, so that red particles must go horizontally. In region B, red particles move freely to the right. In region C, we note that the spectral parameters are of the form of the hypothesis of lemma 9, so that we can apply lemmas 9 and 10 to conclude that the whole region is frozen. The result is that the upper left side of region C reproduces the Young diagram  $\lambda$  read from top to bottom. We now recognize region D as the 180 degree rotated picture of a factorial Schur function (cf section 7.1). Since all tiles and weights are

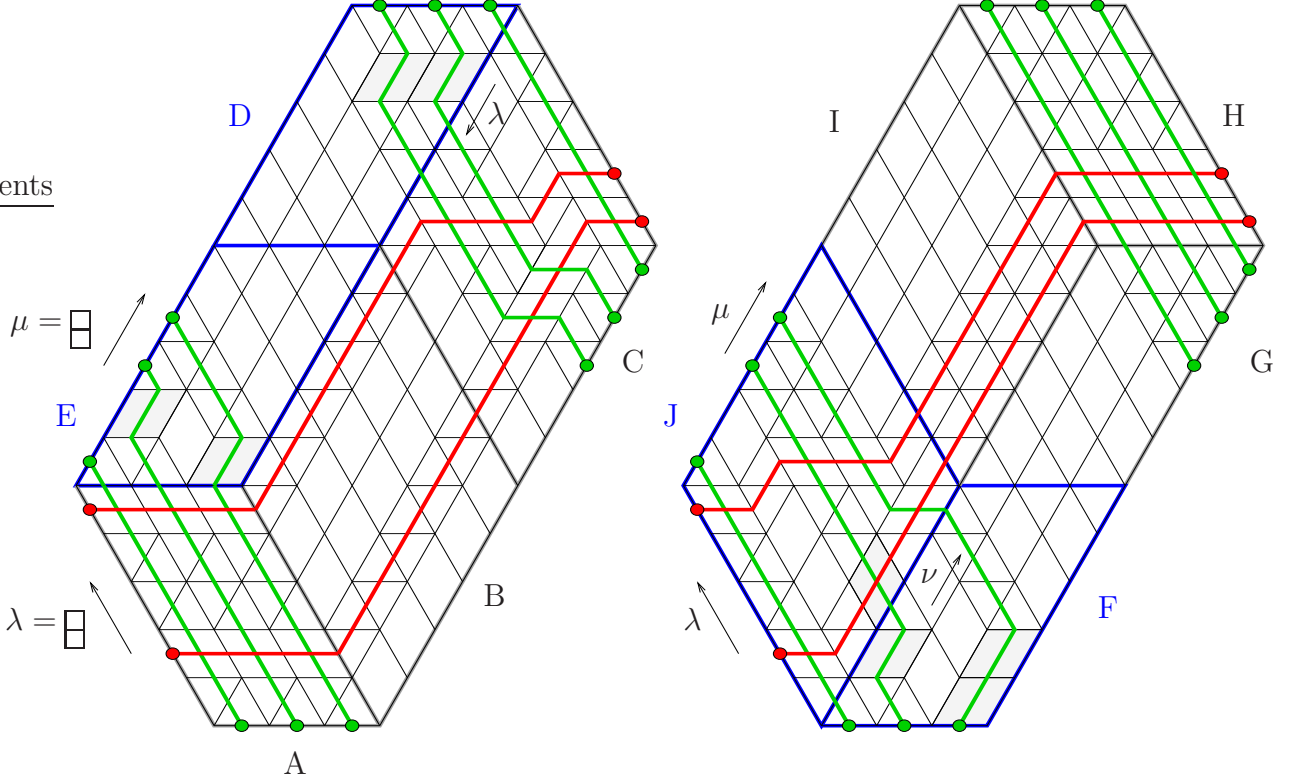


FIGURE 13. An example of tilings contributing to each side of the equality of Fig. 12.

180 degree rotation invariant, we find that this region contributes  $s_\lambda(x_1, \dots, x_k | z_1, \dots, z_n)$ , paying attention to the order of the parameters  $z_i$  (we have however reordered the  $x_i$  because of proposition 2). Region E is the picture of a factorial Schur function with the standard orientation, so it contributes  $s_\mu(x_1, \dots, x_k | y_1, \dots, y_n)$ . Overall, the left hand side equals  $s_\lambda(x_1, \dots, x_k | z_1, \dots, z_n) s_\mu(x_1, \dots, x_k | y_1, \dots, y_n)$ .

Now let us compute the right hand side. In regions G, H and I, it is easy to check that all particles can only move straight in the way indicated on the figure. Region F needs to be dealt with carefully. We want to make sure that the green lines starting from the bottom exit region F through the left side. This requires to look ahead into the region J. Let us consider the rightmost green particle. If we number the upper left side of region J from bottom to top, then its endpoint is precisely  $k + \mu_1$  (the length of the first row of  $\mu$ ). This means that the location (counted from bottom to top) of the rightmost green particle when it crosses the diagonal line starting at the bottom of the junction of J and F cannot exceed  $k + \mu_j$  plus the number of steps to the left it can make in region J. We claim that this number is  $\lambda_1$ : indeed among the  $n - k$  red particles starting from the lower left side of J, only  $\lambda_1$  are allowed to cross without making a step to the right. The last  $n - k - \lambda_1$ , which are the topmost ones, have to make a step to the right each time they cross a green particle in order to reach their final destination to the right of the upper right side of F. The result is that this location is at most  $k + \mu_1 + \lambda_1$ , which by assumption is less or equal to  $n$ . Thus the rightmost green particle, and therefore all others, exit through the left side. We now recognize region F as the factorial Schur function  $s_\nu(x_1, \dots, x_k | y_1, \dots, y_n)$ , where  $\nu$  is the Young diagram, read

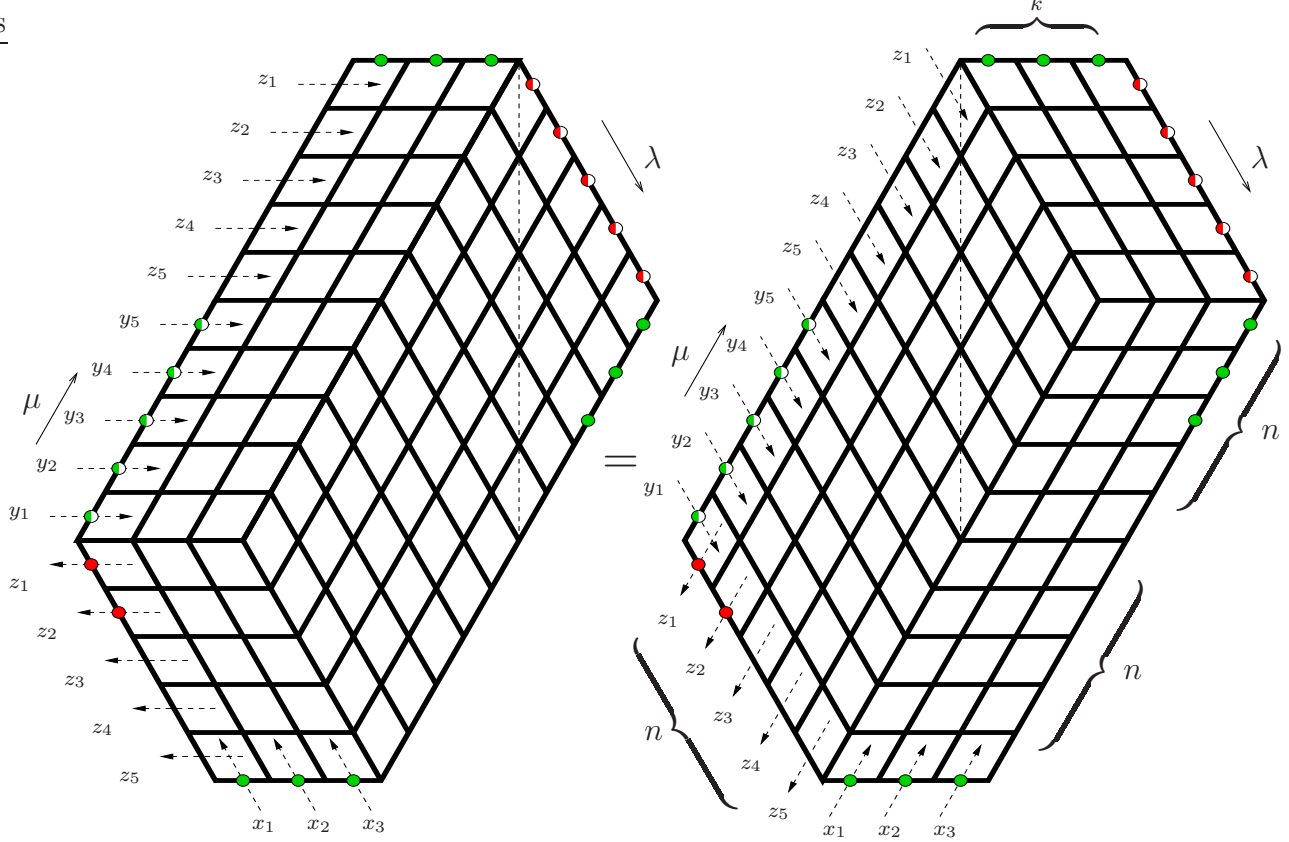


FIGURE 14. Alternate graphical solution of the MS problem ( $n = 5$ ,  $k = 3$ ).

from bottom to top, that encodes the green lines at the boundary between  $F$  and  $J$ . And  $J$  is precisely a MS-puzzle (cf section 7.2), which contributes  $e_{\lambda,\mu}^\nu(y_1, \dots, y_n; z_1, \dots, z_n)$ . So the right hand side equals  $\sum_\nu e_{\lambda,\mu}^\nu(y_1, \dots, y_n; z_1, \dots, z_n) s_\nu(x_1, \dots, x_k | y_1, \dots, y_n)$ .

Finally, we find the desired equality

$$\begin{aligned} s_\lambda(x_1, \dots, x_k | z_1, \dots, z_n) s_\mu(x_1, \dots, x_k | y_1, \dots, y_n) \\ = \sum_\nu e_{\lambda,\mu}^\nu(y_1, \dots, y_n; z_1, \dots, z_n) s_\nu(x_1, \dots, x_k | y_1, \dots, y_n) \end{aligned}$$

The summation over  $\nu$  is only on Young diagrams inside the rectangle  $k \times (n - k)$ , which is related to the fact that (i) we have only  $k$  variables  $x_i$  and (ii) the sum of widths of  $\mu$  and  $\lambda$  satisfies  $\mu_1 + \lambda_1 \leq n - k$ . If one sets all  $y_i$  to zero, then the equality becomes

$$s_\lambda(x_1, \dots, x_k) s_\mu(x_1, \dots, x_k) = \sum_\nu c_{\lambda,\mu}^\nu s_\nu(x_1, \dots, x_k)$$

which is the product formula characterizing the usual Littlewood-Richardson coefficients.

**7.4. Alternate solution of the Molev–Sagan problem.** Interestingly, there is a small variation of the construction of the previous section, which produces another, not obviously equivalent, solution of the Molev–Sagan problem. Since it is based on the same principle, we shall only sketch the derivation, based on Figs. 14 and 15.

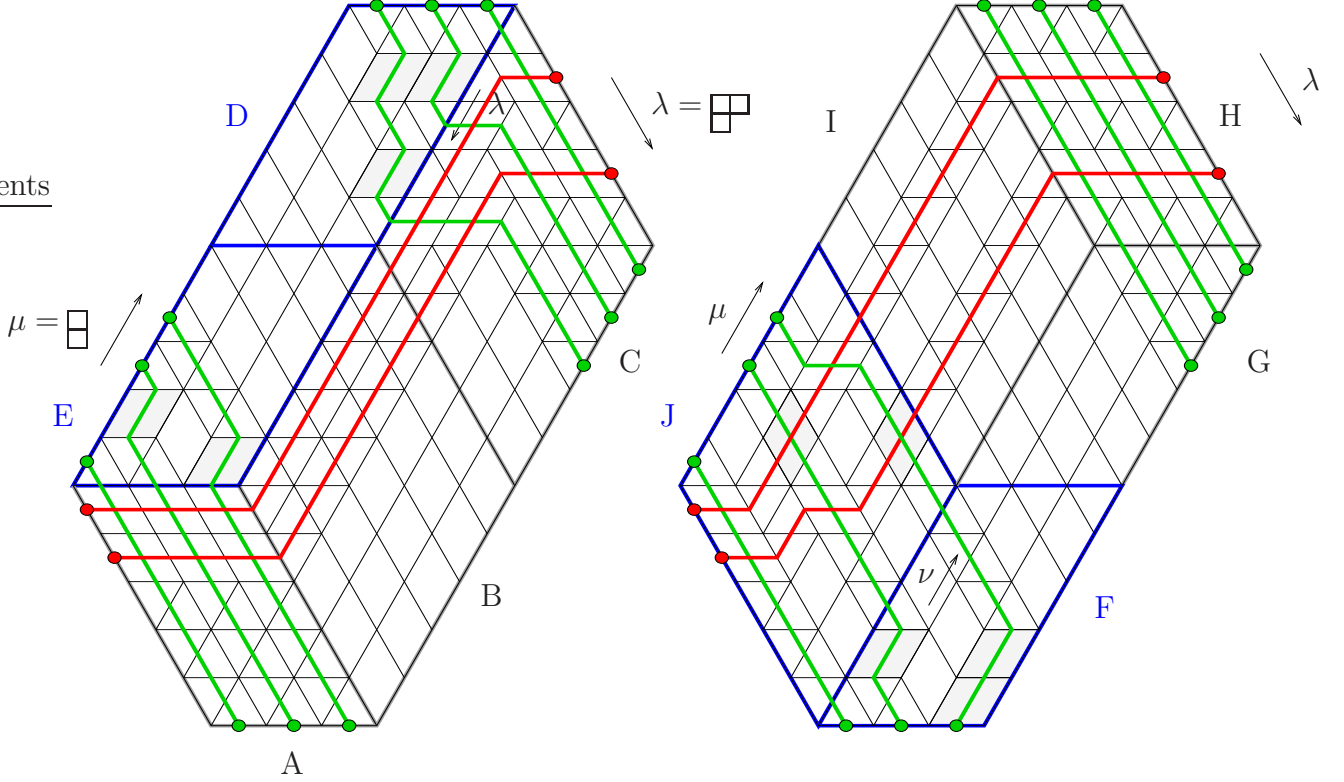


FIGURE 15. An example of tilings contributing to each side of the equality of Fig. 14.

By inspection, one easily finds that regions A, B, G, H, I are frozen, with lines going straight as indicated on the figure. Region C is strictly speaking not frozen; in fact, we recognize an upside-down (180 degree rotated) MS-puzzle, so that its weight is equal to  $e_{\lambda, \emptyset}^{\lambda'}(z_1, \dots, z_n; z_1, \dots, z_n)$  where  $\lambda'$  is the upper left side of C read top to bottom. This, according to the previous section, is the coefficient of  $s_{\lambda'}(x_1, \dots, x_k | z_1, \dots, z_n)$  in the expansion of  $s_{\lambda}(x_1, \dots, x_k | z_1, \dots, z_n) \times 1$  (note the equality of second alphabets!). So it is equal to  $\delta_{\lambda}^{\lambda'}$  (and on the picture we have shown the unique  $\lambda = \lambda'$  configuration).

The other regions are treated the same way as before. Regions D and E correspond to  $s_{\lambda}(x_1, \dots, x_k | z_1, \dots, z_n)$  and  $s_{\mu}(x_1, \dots, x_k | y_1, \dots, y_n)$ . If  $\nu$  encodes as before the edges between F and J, then region F corresponds to  $s_{\nu}(x_1, \dots, x_k | y_1, \dots, y_n)$ , on condition that  $\lambda_1 + \mu_1 \leq n - k$ . Finally region J is an upside-down MS-puzzle with the  $y_i$  in the reverse order, so that we find the equality

$$\begin{aligned} s_{\lambda}(x_1, \dots, x_k | z_1, \dots, z_n) s_{\mu}(x_1, \dots, x_k | y_1, \dots, y_n) \\ = \sum_{\nu} e_{\lambda, \bar{\nu}}^{\bar{\mu}}(y_n, \dots, y_1; z_1, \dots, z_n) s_{\nu}(x_1, \dots, x_k | y_1, \dots, y_n) \end{aligned}$$

As a corollary, we find the curious identity:

$$e_{\lambda, \mu}^{\nu}(y_1, \dots, y_n; z_1, \dots, z_n) = e_{\lambda, \bar{\nu}}^{\bar{\mu}}(y_n, \dots, y_1; z_1, \dots, z_n)$$

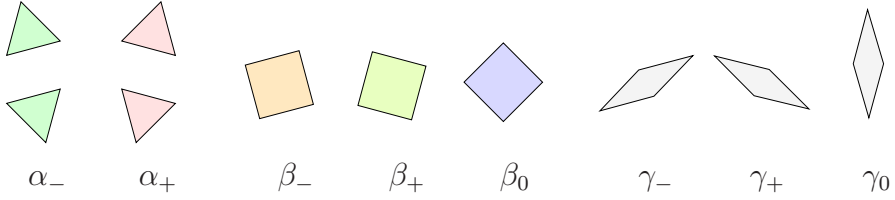


FIGURE 16. Tiles of the square-triangle-rhombus tiling model. The colors are purely decorative.

**7.5. The Knutson–Tao problem.** The Knutson–Tao (KT) problem consists in expanding the product of two factorial Schur functions with the same *two* sets of variables as a sum of factorial Schur functions. It was solved in [10] in terms of equivariant puzzles.

Clearly, a solution of the MS problem provides a solution of the KT problem by setting  $y_i = z_i$ ,  $i = 1, \dots, n$ . Thus, the previous two sections provide two solutions of the KT problem, which turn out to be different. The most interesting one is the alternate one: when  $y_i = z_i$ , the upper half of the rhombus  $J$  of the right hand side of Fig. 15 becomes an equivariant puzzle (as in the example shown), with the spectral parameters labelled in the proper order, and the equality of section 7.4 becomes

$$s_\lambda(x_1, \dots, x_k | z_1, \dots, z_n) s_\mu(x_1, \dots, x_k | z_1, \dots, z_n) = \sum_\nu c_{\mu, \lambda}^\nu(z_1, \dots, z_n) s_\nu(x_1, \dots, x_k | z_1, \dots, z_n)$$

by definition of the  $c_{\mu, \lambda}^\nu(z_1, \dots, z_n)$ , cf section 7.2. This is precisely the formula found in [10].

## APPENDIX A. SQUARE-TRIANGLE-RHOMBUS TILINGS

As mentioned in the introduction, it is known that the tiling model introduced in section 2 is related to the square-triangle tiling model. More precisely, the latter is equivalent to the tiling model without the shaded tiles  $\gamma$ . We describe here the slightly more general (square-triangle-rhombus) tiling model which includes the shaded tiles (in the spirit of [2]). Though it is not needed anywhere in this paper, the connection is worth mentioning.

Consider tiles of three types: equilateral triangles, squares and “thin rhombi” with angles 30 and 150 degrees. All of them have sides of unit length. The square-triangle-rhombus tiling model consists in filling a region of the plane with these tiles, with an addition restriction on the allowed rotations of the thin rhombi which is the following. It is easy to see that all edges can occur in exactly six directions which differ from each other by multiples of 30 degrees. We may for example assume that they are of the form  $15 + 30k$  degrees,  $k$  integer. Thus, there are four possible rotations of triangles, three rotations of square, and six rotations of thin rhombi among which we select only three as shown on Fig. 16.

Now consider the following operation on a given tiling configuration: deform it in such a way that the direction of every edge can only take three values, which is the closest slope of the form  $60k$ ,  $k$  integer. One can show that this can be done consistently (as always in the theory of random and quasi-periodic tilings, these tilings can be seen as projections of a two-dimensional surface embedded in a higher dimensional space – here, four – and

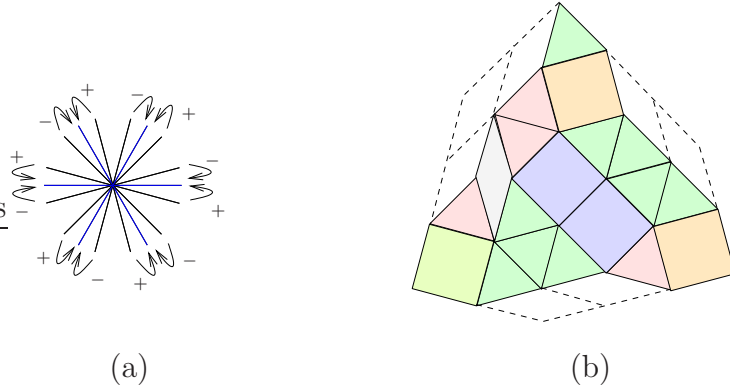


FIGURE 17. (a) The 6 directions of the generalized square-triangle model and how to deform them into the 3 directions (in blue) of the regular triangular lattice. (b) Example of square-triangle-rhombus tiling corresponding to an equivariant puzzle.

the transformation corresponds to changing the direction of projection); furthermore, mark with a  $\pm$  the edge which have been rotated  $\pm 15$  degrees counterclockwise. In this way the triangles become one of the four tiles  $\alpha$  of Fig. 1; similarly, squares become pairs of tiles of type  $\beta$ ; and thin rhombi become pairs of tiles  $\gamma$ . The operation is invertible and is thus the desired equivalence. As before, if we want to preserve integrability, we must allow only one of the three types of thin rhombi in any given region.

For example, starting from Fig. 17 one obtains the equivariant puzzle of the right of Fig. 11. Note that one can read directly the three Young diagrams encoded in the three sides of the triangle (as was observed in [16] in the non-equivariant case), by completing the deformed puzzle into a hexagon with sides of lengths  $k, n - k, k, n - k, k, n - k$  and drawing the complement of the puzzle as sets of the three “forbidden” rotations of the thin rhombi. One must be careful that one recovers this way the three Young diagrams corresponding to the binary strings read *clockwise*.

Another interesting observation is that the use of the Yang–Baxter equation (proposition 1) corresponds in this new language to two elementary operations on tilings (cases (i,ii) and (iii) in the proof), up to reflection and rotation:

$$\begin{array}{c} \text{Diagram 1} \\ = \\ \text{Diagram 2} \end{array} \quad \text{and} \quad
 \begin{array}{c} \text{Diagram 3} \\ + \\ \text{Diagram 4} \\ + \\ \text{Diagram 5} \\ = 0 \end{array}$$

Note the strong similarity with the migration of [16]; the latter is roughly the special case of the Yang–Baxter equation where one spectral parameter is set to zero.

## REFERENCES

- [1] J. de Gier and B. Nienhuis, *Integrability of the square-triangle random tiling model*, Phys. Rev. E **55** (1997), no. 4, 3926–3933.
- [2] ———, *Singular commuting transfer matrices*, unpublished, 2000.
- [3] P. Di Francesco and P. Zinn-Justin, *The quantum Knizhnik-Zamolodchikov equation, generalized Razumov-Stroganov sum rules and extended Joseph polynomials*, J. Phys. A **38** (2005), no. 48, L815–L822, [arXiv:math-ph/0508059](https://arxiv.org/abs/math-ph/0508059), doi:10.1088/0305-4470/38/48/L02.
- [4] ———, *Inhomogeneous model of crossing loops and multidegrees of some algebraic varieties*, Comm. Math. Phys. **262** (2006), no. 2, 459–487, [arXiv:math-ph/0412031](https://arxiv.org/abs/math-ph/0412031).
- [5] S. Fomin and A.N. Kirillov, *The Yang-Baxter equation, symmetric functions, and Schubert polynomials*, Proceedings of the 5th Conference on Formal Power Series and Algebraic Combinatorics (Florence, 1993), vol. 153, 1996, pp. 123–143. MR1394950 (98b:05101)
- [6] I. Gessel and G. Viennot, *Binomial determinants, paths, and hook length formulae*, Advances in mathematics **58** (1985), no. 3, 300–321.
- [7] M. Jimbo and T. Miwa, *Solitons and infinite dimensional Lie algebras*, Publ. RIMS **19** (1983), no. 3, 943–1001, <http://projecteuclid.org/euclid.prims/1195182017>.
- [8] P.A. Kalugin, *The square-triangle random-tiling model in the thermodynamic limit*, J. Phys. A (1994), no. 27, 3599.
- [9] A. Knutson and E. Miller, *Gröbner geometry of Schubert polynomials*, Ann. of Math. (2) **161** (2005), no. 3, 1245–1318. MR2180402 (2006i:05177)
- [10] A. Knutson and T. Tao, *Puzzles and (equivariant) cohomology of Grassmannians*, Duke Math. J. **119** (2003), no. 2, 221–260, [arXiv:math/0112150](https://arxiv.org/abs/math/0112150).
- [11] A. Knutson, T. Tao, and C. Woodward, *The honeycomb model of  $GL_n(\mathbb{C})$  tensor products. II. Puzzles determine facets of the Littlewood-Richardson cone*, J. Amer. Math. Soc. **17** (2004), no. 1, 19–48 (electronic), [arXiv:math.C0/0107011](https://arxiv.org/abs/math.C0/0107011).
- [12] A. Knutson and P. Zinn-Justin, *A scheme related to the Brauer loop model*, Adv. Math. **214** (2007), no. 1, 40–77, [arXiv:math.AG/0503224](https://arxiv.org/abs/math.AG/0503224).
- [13] B. Lindström, *On the vector representations of induced matroids*, Bull. London Math. Soc. **5** (1973), 85–90. MR0335313 (49 #95)
- [14] A.I. Molev, *Comultiplication rules for the double Schur functions and Cauchy identities*, [arXiv:0807.2127](https://arxiv.org/abs/0807.2127).
- [15] A.I. Molev and B.E. Sagan, *A Littlewood-Richardson rule for factorial Schur functions*, Transactions of the American Mathematical Society **351** (1999), no. 11, 4429–4443, [arXiv:q-alg/9707028](https://arxiv.org/abs/q-alg/9707028).
- [16] K. Purbhoo, *Puzzles, tableaux and mosaics*, [arXiv:0705.1184](https://arxiv.org/abs/0705.1184).
- [17] M. Widom, *Bethe Ansatz solution of the square-triangle random tiling model*, Phys. Rev. Lett. **70** (1993), 2094.
- [18] P. Zinn-Justin, *Integrability and combinatorics: selected topics*, Les Houches lecture notes, <http://www.lpthe.jussieu.fr/~pzinn/semi/intcomb.pdf>.

PAUL ZINN-JUSTIN, LPTMS (CNRS, UMR 8626), UNIV PARIS-SUD, 91405 ORSAY CEDEX, FRANCE; AND LPTHE (CNRS, UMR 7589), UNIV PIERRE ET MARIE CURIE-PARIS6, 75252 PARIS CEDEX, FRANCE.

*E-mail address:* pzinn@lpthe.jussieu.fr